Lawrence Berkeley National Laboratory
Recent Work

Title
THE OPTICAL PROPERTIES OF DEFECT STATES IN HYDROGENATED AMDRPHOUS SILICON

Permalink
https://escholarship.org/uc/item/15w5n0tq

Authors
Amer, N.M.
Jackson, W.B.

Publication Date
1983-06-01

eScholarship.org Powered by the California Digital Library
University of California

LBL-16185 c.2

Lawrence Berkeley Laboratory

UNIVERSITY OF CALIFORNIA

ENERGY & ENVIRONMENT DIVISION

RECEIVED
LAWRENCE
BERKELEY LABORATORY
AUG 29 1983
LIBRARY AND
DOCUMENTS SECTION

To be published as a chapter in HYDROGENATED AMORPHOUS SILICON, J.I. Pankove, Ed., Academic Press, New York, NY, Fall 1983

THE OPTICAL PROPERTIES OF DEFECT STATES IN HYDROGENATED AMORPHOUS SILICON

N.M. Amer and W.B. Jackson

June 1983

TWO-WEEK LOAN COPY

This is a Library Circulating Copy
which may be borrowed for two weeks.
For a personal retention copy, call
Tech. Info. Division, Ext. 6782.

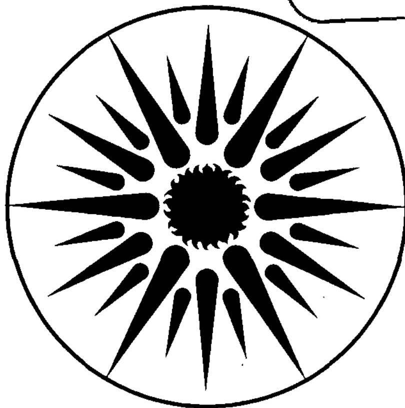

ENERGY
AND ENVIRONMENT
DIVISION

LBL-16185 c.2

Prepared for the U.S. Department of Energy under Contract DE-AC03-76SF00098

DISCLAIMER

This document was prepared as an account of work sponsored by the United States Government. While this document is believed to contain correct information, neither the United States Government nor any agency thereof, nor the Regents of the University of California, nor any of their employees, makes any warranty, express or implied, or assumes any legal responsibility for the accuracy, completeness, or usefulness of any information, apparatus, product, or process disclosed, or represents that its use would not infringe privately owned rights. Reference herein to any specific commercial product, process, or service by its trade name, trademark, manufacturer, or otherwise, does not necessarily constitute or imply its endorsement, recommendation, or favoring by the United States Government or any agency thereof, or the Regents of the University of California. The views and opinions of authors expressed herein do not necessarily state or reflect those of the United States Government or any agency thereof or the Regents of the University of California.

LBL-16185

THE OPTICAL PROPERTIES OF DEFECT STATES IN HYDROGENATED AMORPHOUS SILICON

Nabil M. Amer

Applied Physics and Laser Spectroscopy Group
Lawrence Berkeley Laboratory
University of California
Berkeley, California 94720

and

Warren B. Jackson

Xerox Palo Alto Research Center
Palo Alto, California 94304

June 1983

This work was supported by the Assistant Secretary for Conservation and Renewable Energy, Photovoltaic Systems Division of the Department of Energy under Contract No. DE-AC03-76SF00098 and by the Solar Energy Research Institute Contract No. XJ-0-9079-1.

TABLE OF CONTENTS

I. INTRODUCTION 1

II. PHOTOTHERMAL DEFLECTION SPECTROSCOPY (PDS) 3
A. Physical and Theoretical Basis 3
B. The Experimental Arrangement 7
C. Sensitivity and Comparison with Other Techniques 9

III. OPTICAL SPECTROSCOPY OF DEFECTS IN a-Si:H 11
A. Effects of Deposition and Doping Parameters 11
B. Correlation Energy of Silicon Dangling Bond Defect 15
C. Surface Defects 16
D. Optical Properties of Photo-Induced Defects 17
E. Urbach Edge Studies 20

IV. CARRIER TRANSPORT 21
A. Types of Photoconductivity 22
B. Photoconductivity Results 23

V. PDS-DEDUCED FEATURES IN THE DENSITY-OF-STATES OF a-Si:H 25

VI. CONCLUDING REMARKS 28

ACKNOWLEDGEMENTS 29

REFERENCES 30

FIGURE CAPTIONS 35

The Optical Properties of Defect States in Hydrogenated Amorphous Silicon

I. INTRODUCTION

One of the effects of disorder and doping on the electronic structure of amorphous semiconductors is the introduction of states in the pseudo-gap. These states, commonly classified as defects, significantly affect the properties of the material. Thus, information about their nature, density, and energy is of great interest.

Defects have been extensively studied by luminescence, conductivity, photoconductivity, electron spin resonance, and capacitance techniques. However, these techniques are sensitive to the Fermi-level position, they only detect the radiative component of de-excitation, or they require special doping; hence, they do not measure all defects. Sub-gap absorption, on the other hand, is a fundamental process which measures the energy and number of all defects, thus providing a unique and versatile tool for their study.

Unlike the case of chalcogenide glasses, where optical spectra have been obtained with conventional techniques and the absorption was attributed to transition involving defect centers [1], no direct or reliable spectra were measured in the case of hydrogenated amorphous silicon (a-Si:H). For transmission and reflection techniques to measure the weak absorption associated with gap-states, an accuracy of better than one part in 10^5 in the difference between the incident and transmitted intensities is required. This is clearly beyond the capability of conventional transmission and reflection methods. Consequently, the minimum absorption coefficient (α) which could be measured reliably is 50-100 cm^{-1} for a one-micron thick film [2-7]. The absorption associated with gap-states can be 100 times smaller.

In an attempt to circumvent these difficulties, photoconductivity was employed to deduce the nature of optical absorption in the fundamental gap [8-11]. Photoconductivity, σ, is given by

$$\sigma \propto \eta\mu\tau(1-e^{-\alpha \ell}) \tag{1}$$

where η is the efficiency of generating mobile carriers, μ is their mobility, τ is their lifetime, and ℓ is the material thickness. However, τ is a function of both the generation rate and α, which results in difficulties in deducing α from Eq. (1). Furthermore, to extract α from such measurements requires making the heretofore unverified assumption that $\eta\mu\tau$ product is a constant, independent of the energy of the exciting photons. As shall be seen below, we have shown in recent experiments that, for example, in the case of undoped material, photoconductivity measurements do not yield accurate absorption spectra below 1.5 eV. Localized-to-localized transitions do not contribute to the photocurrent and cause $\eta\mu\tau$ to depend on photon energy.

The limitations of these other methods has motivated us to devise a new approach for measuring small optical absorption coefficients. This approach, photothermal deflection spectroscopy (PDS), is based on measuring the thermal energy deposited in the material of interest as electromagnetic radiation is absorbed. This direct method for measuring the optical absorption proved to be a highly sensitive ($\alpha \ell \sim 10^{-7}$ for solids) and relatively simple tool for material characterization, particularly thin films.

In Section II of this chapter we describe the technique of photothermal deflection spectroscopy. A condensed review of the physics of photothermal generation is given first, with emphasis on those features which are most applicable to the case of a-Si:H films. A detailed description of the experimental arrangement follows. Finally, we compare PDS with techniques

such as conventional absorption and photoacoustic spectroscopies.

In Section III, the optical properties of states in the gap of a-Si:H are reviewed. The effects of deposition parameters, doping, and photo-induced fatigue (Staebler-Wronski effect) on these states and on the Urbach edge will be discussed. Optically derived total correlation energy measurements will be described and compared with those obtained from other techniques, and the contribution of surface defects will be reviewed.

In Section IV, the relationship between photoconductivity and optical absorption is presented, and a discussion of the implications of the energy dependence of the electron and hole $\eta\mu\tau$ product are given. And by combining the results presented in Section III and IV, we sketch in Section V a density-of-states diagram for a-Si:H. Finally in Section VI we summarize the main points of the chapter and speculate on future directions.

II. PHOTOTHERMAL DEFLECTION SPECTROSCOPY

In this section the technique of photothermal deflection spectroscopy [12-14] (PDS) is briefly described. The steps of a comprehensive calculation of the relationship between the optical and thermal properties of the material and the measured signal are outlined. Formulae for the special case of thin films are presented and their limitations are discussed. Details of the experimental setup, signal optimization, and data analysis are given. Finally, we compare PDS with other techniques.

A. Physical and Theoretical Basis of PDS:

The physical principle underlying PDS is straight forward. When an intensity-modulated beam of light (pump beam) is absorbed by a given medium, periodic heating will occur (Fig. 1). The heat from the absorbing material flows into the surrounding medium causing a correspond-

ing modulation in the index-of-refraction near the material surface. A weak laser (probe beam), essentially grazing the material, will experience a periodic deflection synchronous with the intensity modulation. The amplitude and phase of this periodic deflection can be measured with a position sensor and a differential ac synchronous detection scheme. Thus, by varying the wavelength of the pump beam, the deflection of the probe beam is a measure of the optical absorption of the material of interest.

In order to obtain the optical absorption coefficient, the theory of PDS has been developed [12]. We concentrate here on those formulae for temperature, deflection, and detector response which are applicable to the case of thin films.

The derivation of the relation between the optical absorption of the sample and the measured voltage output consists of four steps:

(1) The spatial distribution of the optical energy $I(\vec{r},t)$ is determined within the sample and in the surrounding media. The effect of interference and scattering on the resulting intensity distribution is included at this stage [2,15].

(2) The optical energy is absorbed and the generated heat per unit volume per second is given by $\alpha_f\ I(\vec{r},t)$, where α_f is the extinction coefficient of the film. The heat energy is the source term for the temperature equations which are solved for the material and the surrounding media.

(3) The temperature rise induces an index-of-refraction gradient which deflects the probe beam. The beam deflection is proportional to the heat flow perpendicular to the sample surface across the probe beam.

(4) The detector converts the deflection into a voltage signal which depends on the type of the detector and the experimental geometry.

Following these steps, it can be shown that the deflection signal S is given by [12,15]

$$S = T_r(1/n_o)(dn/dT)L\ (dT(z_o)/dz)e^{i\omega t} + c.c. \tag{2}$$

where T_r is the detector transduction factor (volts/radian of deflection) which depends on the experimental configuration and the detector type. A maximum value is 1×10^3 V/rad. The product $(1/n_o)(dn/dT)$ is the relative index-of-refraction change with temperature for the deflecting medium, L is the length of interaction between the optically heated region and the probe beam, T is the amplitude of the ac temperature rise above the average temperature, z_o is the distance of the probe beam from the sample surface, and *c.c.* denotes the complex conjugate. Since the heat flow is proportional to dT/dz, Eq. (1) demonstrates that the deflection measures the heat flow across the probe beam.

The periodic solution for the temperature in the deflecting medium, the a-Si:H film, and the substrate has the form $T_j \exp(\pm ik_j z - i\omega t) + c.c.$, where $k_j^2 = (i\omega/\lambda_j)$, where ω is the modulation frequency, λ_j is the thermal diffusivity for the *jth* medium, $i = \sqrt{-1}$, and T_j is the complex amplitude of the thermal wave determined from the boundary conditions. The subscript j stands for either d, s, or f which refers to the deflecting medium, the substrate, and the film, respectively. λ_j can be written as $\kappa_j/\rho_j C_j$ where κ_j is the thermal conductivity, ρ_j is the density, and C_j is the specific heat.

The physical interpretation of these solutions is that the temperature can be represented by highly damped waves which decay over the thermal length $1/|k_j|$. These waves experience both reflection and transmission when they propagate through a boundary. The quantity $\kappa_j k_j$ is the "index-of-refraction" of the thermal wave in the *jth* medium. Since the deflection signal is proportional to the heat flow, the deflection measures the flux of thermal waves across the probe

beam path. Specifically, if the film is thermally thin, the temperature gradient is given by

$$dT(z_o)/dz = \frac{k_d \exp(-k_d z_o) I}{\kappa_d k_d + \kappa_s k_s} \begin{Bmatrix} A & \textit{film absorption} & (3.a) \\ -\alpha_d/k_d & \textit{deflecting medium absorption} & (3.b) \\ \alpha_s/k_s & \textit{substrate absorption} & (3.c) \end{Bmatrix}$$

where I is the pump beam intensity ($W.\ cm^{-2}.\ sec^{-1}$), A is the absorptance of the film, and α_j is the absorption coefficient (if any) of the jth medium. Eqs. (2) and (3.a) show that the photothermal deflection is directly related to the optical properties of the film. The terms preceeding the brace in Eqs. (3.a-c) are independent of photon energy and depend only on the thermal properties of the deflection medium and the substrate. At high photon energy, the a-Si:H films are completely absorbing. Consequently, $\alpha_f \ell \gg 1$, $A=1-R_f$, and $S_{sat}=C(1-R_f)$, where ℓ is the film thickness, $R_f(R_b)$ is the reflectance of the front (back) interface, S_{sat} is the saturated PDS signal, and C is a constant composed of factors in Eqs. (2) and (3). For lower photon energies

$$\langle S \rangle = C[1-\exp(-\alpha_f \ell)] \left([(1-R_f)(1+R_b)]/(1-R_f R_b)\right) \quad (4)$$

where <> denotes averaging of the interference fringes on a logarithmic scale (equivalent to geometric averaging). Hence,

$$[1-\exp(-\alpha_f \ell)] = \langle S/S_{sat} \rangle \quad (5)$$

This formula gives the absorptance for an incoherent pump source. In Eq. (5), we assume that the reflectivity factor in the braces of Eq. (4) does not vary significantly with photon energy. The error associated with this assumption is less than 20%. Eq. (5) enables one to determine α_f from PDS alone once the film thickness is known. Additional optical measurements are not needed.

Eq. (5) is valid under the following conditions:

(1) The film is thermally thin $(|k_f|\ell << 1)$. This approximation is valid in the case of a-Si:H since the thermal diffusion length is greater than $50\mu m$ at the intensity modulation used in performing the measurement (7 Hz).

(2) The pump beam should have a radius larger than the thermal diffusion length $1/|k_f|$.

B. The Experimental Arrangement

The experimental set up is shown in Fig. (1). Typically, the pump beam is a 1kW Xe arc lamp focussed on the slit of a ¼ meter monochromator. Various order sorting filters are used to remove unwanted diffraction orders, and the intensity modulation is accomplished with a mechanical chopper operating between 7 and 18 Hz. These modulation frequencies represent a trade-off between a high frequency which is desirable to eliminate the effects of mechanical vibrations and turbulence within the deflecting medium and a low frequency which increases both the thermal diffusion length and the signal amplitude. The pump beam should be focussed as tightly as possible on the film since from Eq. (3.a) the signal is proportional to the intensity (power/unit area) of the pump beam. The probe beam is typically a weak (~ 1 mW) HeNe laser focussed roughly to $75\mu m$ and grazes the film surface. The focal length of the probe beam lens represents a trade-off between a large confocal distance and a small spot size. The deflection of the probe beam is measured by a position sensor [16]. The outputs of the position sensor are amplified by current amplifiers and fed into the (A-B) input of a computer-interfaced lock-in amplifier. The intensity of the pump beam is monitored by splitting off part of the pump beam, before it reaches the film, and detecting it with a pyroelectric detector. The amplitude of the PDS signal is then averaged and normalized by the incident light intensity. The effects of dispersion and residual non-linearities of the system are removed by utilizing a PDS spectrum of

graphite to normalize the a-Si:H spectra. The correction is typically only a factor of two in the 2.1 - 2.6 eV range of the spectrum where the dispersion is largest.

There is a number of other considerations to maximize the sensitivity of PDS: 1) Eqs. (2, 3.a) demonstrate that a figure of merit for various deflecting media is given by

$$F = 1/(n_o \kappa_d)(dn/dT) \tag{6}$$

Since, for a well aligned system, $\exp(-k_d z_o) \simeq 1$ and $\kappa_d k_d > \kappa_s k_s$, if the substrate is SiO_2. In addition, the deflecting medium should have no significant absorption in the photon energy range of interest. Carbon tetrachloride (CCl_4), which has a large F, has an extremely low absorption in the 0.4-2.3 μm range, and ESR measurements show that it does not alter the properties of the a-Si:H films. These consideration make CCl_4 the preferred deflecting medium for a-Si:H studies. 2) The signal is also significantly larger if both the substrate and the deflecting medium have as low as thermal conductivity as possible. Consequently, SiO_2 is superior to Al_2O_3 or crystalline Si. 3) The probe beam should be as close to the film surface as possible so that $\exp(-k_d z_o) \simeq 1$. This requires the sample to be placed on a micrometer-driven translation stage to adjust the distance between the probe beam and the sample. In addition, it is desirable that the sample holder has a rotational degree of freedom to allow the probe beam to be close to the sample, without being eclipsed. 4) Particular care should be taken to keep the deflecting fluid free from particulates as they can be a significant source of noise. 5) The pointing stability of the probe laser can be the factor limiting the sensitivity of the technique. 6) To eliminate air currents, the optical paths should be suitably enclosed.

C. PDS Sensitivity and Comparison with Other Techniques

PDS is a highly sensitive technique with numerous advantages over traditional reflection and transmission and photoacoustic methods. A detailed comparison is discussed in Ref. [12]. In this section we discuss the sensitivity and compare aspects of PDS to other techniques which have been employed in studies of amorphous materials.

The PDS sensitivity which can be achieved routinely with monochromatic broad band sources is 1×10^{-8} W of absorbed power. Since typical available powers are on the order of ~ 1 mW at 0.8 eV, an absorptance of 10^{-5} can be readily measured. For a 1 μm film, α's as low as 0.1 cm^{-1} at 0.8 eV can be determined. The sensitivity is limited by the probe beam stability, turbulence, and scattering from particles in the deflecting medium. Furthermore, at this level of sensitivity, absorption by the substrate material can be a sensitivity-limiting factor. Almost all SiO_2 has a surface absorbing region with an absorptance of $\sim 10^{-5}$, [17] in addition to the O-H overtone absorption band at 1.38 μm. This background may be minimized by using OH-free glass and by monitoring the signal phase. Nevertheless, it does place a limit on the ultimate achieved sensitivity. It should be noted that if the pump beam is a tunable laser, the signal-to-noise ratio increases because of the higher power and smaller beam spot size.

It is instructive to write the PDS signal in terms of film surface temperature rise, $\tau(o)$, integrated over the optically heated area so that the sensitivity may be compared with that of photoacoustic spectroscopy. Eq. (2) can be evaluated to give $S \simeq 10\ V cm^{-2} \cdot C^{-1} \tau(o)$. In the case of photoacoustic detection, the corresponding factor is $0.1\ V\ cm^{-2} \cdot C^{-1} \tau(o)$. Hence, PDS is approximately 100 times more sensitive than photoacoustic spectroscopy.

One of the strengths of PDS over other techniques is that the background signal (e.g., signal due to substrate absorption) is small and can be easily separated out from that due to the

film absorption. This is not the case for conventional absorption techniques. Eqs. (3.b) and (3.c) indicate that one can distinguish between the substrate and deflecting medium absorption by utilizing the signal phase information. The substrate produces a signal with a lagging phase of 45° while the deflecting fluid signal will be leading by a phase of 135° with respect to that of the mechanical chopper. This ability to determine the source of absorption is extremely important in low absorption measurements since substrates such as quartz and pyrex glass are known to have weak surface absorption [17].

The effects of elastically scattered light are much less significant for PDS than for both photoacoustic spectroscopy and transmission techniques. In transmission techniques, the scattered and absorbed light are not separable, so the measured extinction coefficient is often considerably larger than the actual coefficient. In PDS, light scattered elastically from the bulk will not contribute to the signal unless it is scattered along the probe beam and is subsequently absorbed. Since this event is unlikely, PDS is highly insensitive to scattering [15]. Also, PDS is less sensitive than photoacoustics to scattering from surface inhomogeneities, since the scattered light must be absorbed near the probe beam. Photoacoustic also has a background signal due to scattered light striking the photoacoustic cell and/or the microphone detector. In PDS, the probe beam may be blocked to determine if stray light is falling on the position sensor. Such light may be filtered out by the use of a HeNe laser line filter to eliminate this background. Throughout our investigations on various a-Si:H films, we found that PDS is largely insensitive to scattering except in the case of mechanically roughened samples.

III. OPTICAL SPECTROSCOPY OF DEFECTS IN a-Si:H

As in crystalline semiconductor, factors determining the electronic structure and the density of states in a-Si:H are of fundamental and practical interest. While some states, localized and extended, occur in the material regardless of the method and parameters employed in making the films, others are introduced during the deposition process. The nature and number of these extrinisic states, usually called "defects", is a strong function of the deposition parameters and the type and level of doping. Furthermore, even after the deposition of the material, exposure to light introduces metastable defects which are annealed away by heating. Although the intrinsic states are of interest, we concentrate our coverage in this chapter on those extrinsic states which we defined earlier as "defects."

A. The Effects of Deposition and Doping Parameters:

Traditionally, the convention is to divide the optical absorption edge of amorphous semiconductors into three regions: a) a power law region; b) an exponential absorption edge, often called the "Urbach edge"; and c) a tail which extends, beyond the Urbach edge, into the pseudo-gap. The latter two regions are known to be sensitive to defects in crystalline semiconductors.

Figs. (2) shows the effect of substrate temperature on the optical absorption spectrum in regions (b) and (c) as obtained by photothermal deflection spectroscopy. The subgap absorption is lowest for material deposited at 230°C and increases for both lower and higher deposition temperatures. The effect of increasing the deposition power density on the subgap absorption for a constant substrate temperature is given in Fig. (3). Again, deposition conditions known to produce large defect densities and columnar growth yield a discernible shoulder at $\sim$ 1.25 eV. A second pronounced effect is the progressive decrease in the slope of the exponential edge as the

deposition conditions depart from optimal [18-19]. Finally, if undoped films, deposited at low substrate temperatures, are annealed, subgap absorption first decreases as the annealing temperature is increased to ~300°C, then increases again for temperatures higher than 300°C [20].

The effects of single doping and compensation [21] are shown in Fig. (4). The spectra for various phosphorous doping levels are summarized in Fig. (4a). The gap-state absorption increases and the Urbach edge broadens as the phosphorous concentration is increased. Boron doping has a similar qualitative effect on the absorption spectrum (Fig. 4b). However, the change in the slope which differentiates between the Urbach edge and the subgap absorption becomes less pronounced than is the case for phosphorous doped material.

The changes due to the introduction of dopants can be caused either by a shift of the Fermi level or by the bonding configurations of the dopant atoms. These effects can be separated by investigating compensated (simultaneous incorporation of n and p type dopants) materials. The results from a series of studies on compensated material are shown in Fig. (4c). The films were prepared by fixing the PH_3 concentration and gradually increasing the B_2H_6 vapor pressure. As the boron concentration increases, the magnitude of the gap-state absorption decreases. Concurrently, the Urbach edge broadens and shifts to lower energies.

The results in Figs. (2-4) demonstrate that the subgap region is highly sensitive to doping and to deposition conditions. From the subgap absorption, information about the nature, energy, and number of defects in a-Si:H can be obtained.

The number of defects can be estimated by separating the subgap defect absorption from the exponential band tail absorption. The excess optical absorption (α_{ex}) due to gap-state defect absorption is given by

$$\alpha_{ex} = \alpha - \alpha_o \exp[\hbar\omega / E_o] \tag{7}$$

where α_o and E_o are obtained from a fit to the exponential absorption.

From an optical sum rule, the number of defects (N_s) is related to the absorption by

$$N_s = \frac{cnm}{2\pi^2\hbar^2 e_s^{*2}} \int \alpha_{ex}(E) dE \tag{8}$$

where c is the speed of light, n ($\simeq$ 3.8) is the index-of-refraction of silicon, m is the electron mass, and e_s^* is the effective charge of the defect [22]. The integration limits extend from zero to the energy where the exponential absorption terminates ($\sim$1.3—1.6 eV). Using the local field corrections employed in interpreting the infrared absorption spectra of a-Si:H.[22,23], e_s^{*2} is given by

$$e_s^{*2} = \frac{9n^2}{(1+2n^2)^2} e^2 f_{oj} \tag{9}$$

where f_{oj} is the oscillator strength of the absorption transition and e is the electron charge. Assuming f_{oj} = 1 and noting that the local field corrections have been determined to overestimate the correct local field by a factor of 2 in a-Si:H, [22,24] then

$$N_s = 7.9\text{x}10^{15} \int \alpha_{ex} dE \tag{10}$$

Eq. (10) provides a useful measure of the relative number of defects in the a-Si:H. The assumptions that f_{oj} = 1 and that the integration terminates at $\sim$1.5 eV need to be verified by comparing the number of defects obtained from Eq. (10) with those measured by other techniques such as electron spin resonance (ESR), light-induced ESR (LESR), and luminescence.

The dominant defect in undoped a-Si:H is an ESR active defect with a g-value of 2.0055, characteristic of a silicon dangling bond [25]. By comparing the number of dangling bonds determined by ESR with N_s as measured by PDS, it is found that the numbers agree extremely well over three orders of magnitude (see Fig. 5). This excellent agreement shows that the subgap absorption in undoped material is due to singly occupied silicon dangling bonds. It should be noted that, in addition to yielding the absolute number of dangling bonds, PDS is more sensitive to smaller dangling bond densities than ESR. The linear relation between the absorption and the dangling bond density is unlike the case of unhydrogenated amorphous silicon where the number of the absorption-derived defects vary as the square of the number of ESR-measured spins [26].

In the case of phosphorous doping, the silicon dangling bonds are doubly occupied, while for boron doped material the dangling bond is unoccupied. Consequently, the defects are LESR-active with a dangling bond g-value of 2.0055. The number of these defects may be determined from LESR or deduced from the quenching of the luminescence [25]. There is s good correlation between N_s and the number of doubly occupied and the unoccupied dangling bonds as shown in Fig. (6). This is a clear evidence that the silicon dangling bond defect is the source of gap-state absorption in doped a-Si:H as well. Eq. (10) appears to underestimate the number of defects in boron doped material. This is most likely due to the fact that subgap absorption, in the case of boron doping, overlaps with the band-to-band transitions responsible for the exponential tail absorption. To compensate for this, the limits of integration should be extended by ~0.1 eV.

Fig. (6) demonstrates that the defect density varies as the dopant concentration is increased. From PDS, LESR, and photoconductivity measurements, it is found that the defect

density varies as the square root of the dopant concentration [27]. Consequently, by combining the sensitivity of PDS with the square root dependence, very low doping concentrations can be measured readily. Recently, PDS results from doped material were invoked in a model to explain doping in a-Si:H [27]. Because of uncertainties in photoconductivity, luminescences, and LESR measurements, PDS gives the most reliable estimates of defect densities in doped material.

In addition to measuring the number of defects, PDS may also be used to determine the energy of the silicon dangling bond defects. The absorption coefficient is given by

$$\alpha\hbar\omega \propto M^2 \int_{E_{F-\hbar\omega}}^{E_F} N_V(E) N_c(E + \hbar\omega) dE \tag{11}$$

where M is the transition matrix element, $N_V(N_c)$ is the density-of-states below (above) the Fermi level E_F. M is assumed to be independent of energy. Using the density-of-states discussed in Sec. V, the energy dependence of the absorption coefficient may be fitted to the data with an adjustable peak position. Then best fit is obtained for a peak position of approximately 1.25 eV and 0.9 eV below the conduction bond for undoped and phosphorous doped materials, respectively.

B. The Correlation Energy of Silicon Dangling Bond Defect

Using PDS, the energies of the singly and doubly occupied dangling bond defects can be compared to give a measure of the electronic correlation energy of the defect.

The total energy required to place a second electron on the dangling bond is the sum of the Coulomb repulsion and the dielectric and atomic relaxation energies. If the sum is positive, the doubly occupied dangling bond will be closer to the conduction band. Consequently, gap-state

absorption will exhibit a threshold at a lower energy, otherwise it remains unchanged. By comparing the singly and doubly occupied dangling bonds in undoped and phosphorous doped material, respectively, it is found that the absorption of the doped films is shifted to lower energies by ~0.35 eV (Fig. 8). Hence, the correlation energy U of the silicon dangling bond defect is positive and has a value of ~0.35 eV, [28] which agrees with the value deduced from the ESR study of the dependence of the number of spins on the Fermi level position [29]. The fact that U is positive implies that the coulomb repulsion dominates. The implication of these results to the density-of-states are discussed in Sec. V.

C. Surface Defects

There is significant evidence for the existence of surface and interface defects in a-Si:H films. Such evidence comes from ESR [30], photoconductivity [31], and conductivity [32,33] measurements. However, ESR requires the use of relatively thick films, and both ESR and conductivity measurements are inherently unable to differentiate between actual changes in the density-of-states and band bending and/or Fermi level shifts. PDS, with its high sensitivity, enables one to measure the total density of defects over a wide range of film thickness. This would provide a measure of the density of surface defects independent of the Fermi level position.

By combining Eq. (10) with the PDS results of a thickness dependence study [34], it was found that, for low defect material, the film surface (or its interface with the substrate) has a defect density of $\sim 10^{12}$ silicon dangling bonds/cm^2 (Fig. 9). The results also indicate that the defects are confined to a very thin (5 nm) surface or interface layer. The absorption spectra of the defective layer are similar to those obtained from the highly defective bulk a-Si:H (high gap state absorption and broadened Urbach edge). This indicates that the bulk density-of-states is

different from that at the surface (or interface). It also explains why field effect measurements, which are surface sensitive, consistently yield larger densities of gap-states than those obtained by capacitance transient measurements.

D. Optical Properties of Photo-Induced Defects

The reversible photo-induced changes (Staebler-Wronski Effect) in the properties of a-Si:H have attracted much attention [35,36]. Illumination creates metastable defects which are annealed away by heating the films above 150°C. However, the exact mechanism responsible for this effect remains to be elucidated.

An interesting question is how does the so-called "Staebler-Wronski Effect" affect the absorption spectrum of states residing in the gap of a-Si:H. Furthermore, although ESR measurements suggest an increase in the number of silicon dangling bonds after illumination, these studies detect unpaired spins only. Therefore, it is possible that the density of dangling bonds remains constant and the observed increase would then be due to a shift in the Fermi level deeper into the gap, in a region of increased dangling bond states. In this case, the number of unpaired spins would increase eventhough the total number of dangling bond defects remains constant.

Fig. (10) shows the effect of illumination with broadband light on the gap state absorption of an undoped sample. The spectra show a clear and reproducible enhancement in gap-state absorption after illumination. Annealing at 150°C, in the dark, restores the magnitude of the absorption to its original value. The spectra of the annealed and illuminated films are qualitatively similar, with the only difference being the higher magnitude of the sub--gap absorption. Using the procedures described in Sec. III.A, the density and energy position of the optically-induced defects can be determined [37].

In the case of undoped material, the increase in gap-state defect density, ΔN_s is found to be constant ($\sim 10^{16}$ defects/cm^3, in agreement with ESR results [38]), irrespective of the preparation conditions. The dependence of ΔN_s on doping level is shown in Fig. (11). The ratio $\Delta N_s / N_s$ is found to be roughly constant, indicating that the photoinduced defects scale with the doping-induced defect concentration (Fig. 12). In the case of the fully compensated material, ΔN_s showed the least enhancement. Using Eq. (11), the energy of the defect is found to be 1.25 eV and 0.9 eV below the conduction band for undoped and phosphorous doped films, respectively.

The PDS spectra show no change in the Urbach edge, which in the case of a-Si:H is dominated by the valence band edge [39]. Another experimental tool for probing the edge is photoinduced absorption where the shape of the valence band tails determines the rate of the photoexcited carrier decay [40]. No change was found in the decay rate between the illuminated and the annealed states. One can then conclude that the photoinduced defects do not alter the shape of the valence-band tail [41]. Both the PDS and the photoinduced absorption results are not consistent with an increase in the number states near the valence band edge [42].

Several significant conclusions can be drawn from these results. The observed enhancement in dangling bond defects upon illumination is due to the creation of new defects and not caused by Fermi level shift towards midgap. A shift in the Fermi level to lower energy, alone, would result in less absorption rather than an increase, as observed experimentally. Furthermore, the successive increase in dopant concentration moves the Fermi level into the band tails. It will then be in a region of the density-of-state diagram with smaller dangling band density; consequently, the detected effect should decrease with increased doping. However, as seen in

Fig. (11), the photo-induced change in defect density increases with doping. One is then led to conclude that illumination creates new silicon dangling bond defects [43].

Since ΔN_s is constant in the undoped material, independent of deposition parameters, this implies that photoinduced defects may be related to impurities rather than weak silicon-silicon bonds. Preliminary results [43] with films of grown with large oxygen content tend to confirm the conclusion that impurities may be involved. The constant ratios $\Delta N_s / N_s$ for singly doped films, independent of the type and concentration of the dopant, and of the film thickness, indicates that the photoinduced states are themselves related to defects associated with doping. Finally, compensation with equal amounts of phosophorous and boron has the striking effect of drastically minimizing N_s. This suggests that the position of the Fermi level may be important in determining the number of photoinduced defects.

The results can also be used to shed some light on the mechanism responsible for creating the photoinduced defect. The data imply that such a mechanism does not involve breaking Si-Si bonds. The scaling of ΔN_s with doping can be attributed to increased local strain. Furthermore, high defect density undoped material has a large number of weak Si-Si bonds due to strain disorder. Yet ΔN_s is constant, independent of the degree of disorder. Thus, the photoinduced defects are not related to strain disorder, and this, in turn, suggests that weak Si-Si bonds are not primarily involved in the defect creation.

In the context of solar cell technology, the PDS results have some practical implications. When air is leaked into the deposition chamber, solar cells exhibit an even greater drop in efficiency after illumination, which can be annealed away by heating [44]. The conclusion that photo-induced defects are impurity-related is consistent with this observation. In addition, it is known that for heavily doped p-i-n solar cells, illumination results in a fall-off in the blue

response of the cell [35,45,46]. In this case, the heavily doped outer layer will have the largest density of light-induced defects. Consequently, only the photons with short penetration depths will be strongly affected.

E. Urbach Edge Studies by PDS

A full treatment of the exponential edge absorption involving band-to-band transitions is given in Chapter 1. In this section we review results obtained with PDS [19] in conjunction with the work discussed in Section III.A. From Figs. (2-4) it is evident that the slope of the exponential edge depends on the conditions under which a-Si:H is prepared as well as on the type and degree of doping. As the number of defects increases, the Urbach edge broadens.

The absorption edge in that region can be fitted to the form

$$\alpha=\alpha_o \exp(\hbar\omega/E_o) \tag{12}$$

where E_o is the width of the exponential edge. To test the degree of correlation between the width of the edge and the number of defects, E_o is plotted in Fig. (12) as a function of the equilibrium spin density. A strong correlation is found, with the functional form $N_s \propto \exp(E_o/10\ \mathrm{meV})$, that could be interpreted as evidence that the disorder-induced fields and strains responsible for controlling the slope of the Urbach edge are caused by dangling bond defects. Alternatively, the defects and the structural disorder may be produced concurrently while the material is being deposited.

The optical absorption edge of a-Si:H is dominated by the band with the broadest exponential tail, i.e., the valence band tail [39]. Photoinduced absorption studies [40] have been

assumed to measure this part of the density of states diagram. Photoinduced absorption $\Delta T_r/T_r$ is given by

$$\Delta T_r/T_r \propto t^{-\beta} \qquad (13)$$

where $\beta = T/T_o$, $T_o = E_o/k_B$, and k_B is the Boltzman constant. As shown in Fig. (14), an excellent correlation is found between E_o from PDS and from photoinduced absorption. Therefore, this strong correlation verifies the assumption that the shape of the valence band tail determines the rate of photoinduced absorption decay.

IV. CARRIER TRANSPORT

In the previous sections, PDS was used to determine the optical absorption of a-Si:H. This technique may also be employed to measure transport properties as well. Because photoconductivity (PC) depends on both the absorption and carrier transport, the combination of PDS and PC provides information about the dependence of the carrier transport on excitation energy [47]. In addition PDS, also provides a way of normalizing the photoconductivity to account for effects of intensity on the carrier lifetime [47]. A complete review of the various aspects of photoconductivity is given in Chapter 8.

Disorder significantly alters the transport of carriers. Within the bands, the carriers occupy extended states while within the gap, the states are localized. Consequently, the distance a carrier moves in a field, the range, should show a decrease as the energy of the exciting light is decreased. The range per unit field is given by $\mu\tau$ where μ and τ are the carrier mobility and lifetime, respectively. Comparison of PC and PDS has shown that there is a fairly rapid transition from extended to localized transport.

A. Types of Photoconductivity

Three different configurations are used for measuring PC and depend on different aspects of carrier transport. If PC is measured with a gap electrode configuration, the photocurrent depends on the transport of both the electrons and the holes (Fig. 15). The electrodes can inject both electrons and holes to maintain the charge neutrality of the films. The resulting photocurrent, ΔI_{ss}, is given by

$$\Delta I_{ss} \propto [(\eta\mu\tau)_e + (\eta\mu\tau)_h] f \tag{14}$$

where η is the efficiency of carrier generations and the subscripts e and h refer to the electron and hole, respectively. The average number of photons absorbed per cubic centimeter per second, f, is given by

$$f = \Phi S / \ell S_{sat} \tag{15}$$

where Φ is the flux of photons per cm^2 per sec, S is the photothermal deflection signal, and ℓ is the film thickness.

If the photocurrent is measured on a forward biased Schottky barrier, the electrons can be injected by the back contact while the holes cannot be injected by the Schottky barrier. Consequently, the photocurrent, ΔI_{sp}, depends only on the electron transport and is proportional to

$$\Delta I_{sp} \propto f\,(\eta\mu\tau)_e \tag{16}$$

Finally, if the photocurrent is measured on a reverse biased Schottky barrier, neither electrode can inject carriers. When the film is thick and the carriers are excited by subgap light, the photocurrent is given by

$$\Delta I_{pp} \propto (\eta\mu\tau)_h f \tag{17}$$

Eqs. 16 and 17 indicate that in principle, $(\eta\mu\tau)_e$ and $(\eta\mu\tau)_h$ can be determined using photoconductivity. Unfortunately, $\eta\mu$ may depend on the photon energy and τ depends on the generation rate, f, which also depends on photon energy. The PDS measurements allow one to adjust the incident light intensity to hold f constant and hence to eliminate the f dependence of τ. Dividing the constant generation rate normalized PC spectra by the PDS spectra gives energy dependence of $(\eta\mu\tau)_e$ and $(\eta\mu\tau)_h$ at equilibrium due to changes in the photon energy.

B. Photoconductivity Results

The results of the three different kinds of photoconductivity measurements and PDS for an undoped film is shown in Fig. (16). At the high energies above 1.6 eV, the spectral dependence of the four measurements is the same. Below ~1.5 eV, the reversed biased Schottky photocurrent begins to deviate from other measurements. Finally, at ~0.9 eV, the absorption differs from the gap electrode and forward biased Shottky photocurrents.

These results are explained by considering the density-of-states discussed in Sec V. For photon energies greater than ~1.6 eV, both photogenerated carriers are either mobile or can thermalize at room temperature during their lifetime. The spectral dependence of the three photocurrents follow the absorption indicating that $(\eta\mu\tau)_e$ and $(\eta\mu\tau)_h$ are independent of energy (Fig. 16). Below ~1.5 eV, a hole cannot thermalize the valence band edge. The photocurrent of reversed biased Schottky barrier decreases relative to the absorption. The dotted line in Fig. (16) shows the dependence of the reverse biased Schottky barrier after corrections for internal photoemission [47]. Because the electron current dominates the hole current in undoped and phosphorus doped films, the gap cell and forward biased Schottky photocurrents will follow the

absorption since the electron is still mobile. $(\eta\mu\tau)_h$ shows a rapid decrease while $(\eta\mu\tau)_e$ remains constant (see Figs. 17, 18). For energies less than 1.0 eV, neither the electron nor the hole are mobile, leading to a deviation between the gap electrode and forward biased Schottky photocurrents and the absorption. $(\eta\mu\tau)_e$ exhibits a decrease especially in the phosphorus doped case.

The fact that $(\eta\mu\tau)_e$ is roughly constant to 0.9 eV, demonstrates that the defect absorption transition results in the same final state as band-to-band transitions. Consequently, the defect absorption is due to transitions from the defect to the conduction band rather than from the valence band to the defect. The energy threshold of the defect absorption measures the energy of the defect relative to the conduction band.

The results also indicate that geminate recombination is not the dominate recombination path. Otherwise $(\eta\mu\tau)_e$ and $(\eta\mu\tau)_h$ would show a large decrease for photon energies less than 1.6 eV. Due to the large error bars, the possibility that a small fraction of the photocarriers recombine geminately cannot be excluded.

The comparison of PDS with PC indicates that while in principle PC can be used to determine the absorption, in practice, the variation of the carrier lifetime with intensity causes distortions in the energy dependence of the photoconductivity. Empirically, it has been found that after careful normalization, the defect absorption may deviate by as much as a factor of 2-3 relative to the above band value. Hence, the photoconductivity derived absorption slopes are uncertain by about 15 meV.

PDS can be used to normalize photoconductivity since the lifetime is a function of the generation rate. If the photocurrent is measured as a function of light intensity, one obtains the functional dependence of the lifetime on generation rate. Using the absorption from PDS and the measured light flux, one can determine the generation rate to derive the photocurrent at a

constant generation rate (and hence lifetime). This technique enables one to use photoconductivity in situations where PDS is unsuitable due to background absorption.

The results presented in this section demonstrate the versatility and utility of PDS. Not only can the optical absorption be measured but the range of photoexcited carriers can be determined as well.

V. PDS-DEDUCED FEATURES IN THE DENSITY-OF-STATES of a-Si:H

In this section, the contributions of PDS to the understanding of the density-of-states in a-Si:H are described, and the results mentioned in the previous sections will be placed in a more comprehensive picture.

The density-of-state diagram, as deduced from a variety of techniques including photoemission, dispersive transport, photoinduced absorption, deep level transient spectroscopy (DLTS), luminescence, and ESR as well as PDS, is shown in Fig. (19) for undoped and phosphorus doped a-Si:H. First consider the conduction band. Little is known about the bottom of the conduction band near the band-gap other than it is probably close to a parabolic density-of-states and possesses no sharp structure [48]. Comparison of derived absorption spectra to PDS spectra suggest that the conduction band may be somewhat broadened compared to $(E-E_c)^{1/2}$, however, more experiments need to be performed.

Near the conduction band edge, the states become localized below the conduction band mobility edge, E_c. The comparison of the absorption to the photoconductivity support the view that the states become localized near the conduction band edge. Below the mobility edge, dispersive transport has shown that the states tail exponentially into the gap. The edge is extremely sharp, decreasing by 5 orders of magnitude in 0.25 eV. An important consequence of

the rapid decrease of the conduction band tail is that the spectral dependence of the absorption is dominated by the energy distribution of the valence band and defects states, rather than being a mixture of features of the conduction and valence band density-of-states.

In the energy range of 0.7—1.5 eV below the conduction band, the density-of-states is dominated by silicon dangling bond defects. The correlation of the spin density with the gap-state absorption provided first evidence that a peak in the density-of-states, located slightly below midgap at ~1.25 eV below the conduction band was specifically associated with the silicon dangling bond [18,19]. This peak grows as the rf power increases, if the substrate temperature deviates from 180—250°C, or if the film is annealed to remove hydrogen. The integrated magnitude of the dangling bond peak ranges from roughly from 10^{15} to 10^{19} states cm^{-3}. The integrated magnitude of the dangling bond peak increases to ~10^{17} states cm^{-3} near the interface and/or surface. The spatial inhomogeneity explains the descrepancy between the interface sensitive field-effect measurements of the density-of-states and the bulk sensitive capcitance DLTS measurements. The singly occupied dangling bond defect peak increases by 10^{16} states cm^{-3} if the films are exposed to above band-gap illumination for protracted time.

Phosphorus doping causes the dangling bond defect peak to increase in magnitude as the square root of the doping concentration and to move to a higher energy (+0.38 eV) due to the Coulomb replusion between the two localized electrons on the dangling bond. Boron doping also increases the defect concentration as the square root of the doping concentration. It should be noted that, since the spectral dependence of the photoconductivity and PDS has not been performed on boron doped material, it is not known whether the peak lies close to the conduction band or near the valence band. Finally, compensation decrases the dangling bond defect peak.

The effect of illumination is to increase the magnitude of the dangling bond peak by ~30% in both phosphorus and boron doped samples. By a mechanism not yet understood, the number of photo-induced defects is related to the number of defects which previously existed prior to illumination. The process apparently involves the position of the Fermi level since the compensated material exhibits a very small increase.

The valence band edge decreases exponentially into the gap from the valence band mobility edge. The width of the valence band is very sensitive to deposition conditions and doping. Many parameters which increase the dangling bond defect density also increase the width of the valence band tail, roughly according to the relation $N_s \propto \exp(E_0/10\ \mathrm{meV})$. However, if the dangling bonds are photoinduced, an increase in the valence band tail does not occur. This fact suggests the possibility that disorder, as measured by the valence band width, causes dangling bonds during deposition. Apparently, the photo-induced dangling bonds do not by themselves cause disorder of the tail above the valence mobility edge.

Comparison of the spectral dependence of the hole current to the absorption indicates that, at least over the range of tenths of an eV, the hole states make a transition from extended to localized behavior. The width of the transition cannot be determined accurately because the measurements were performed at high temperatures and the internal photoemission causes a large background. The photoconductivity measurements on Schottky barriers demonstrate that the optical transitions occur between filled defect states and the conduction band for undoped and phosphorus doped material.

VI. CONCLUDING REMARKS

The preceeding discussion demonstrates the utility of using PDS to obtain information about the density-of-states in a-Si:H. The power of measuring optical absorption arises from the fact that it is a fundamental and well understood process occurring in all solids. Typically, absorption measurements do not require contacts, doping conditions, Fermi level positions, special temperatures, device structures, etc. The effect of almost any material parameter on the density-of-states can be assessed by measuring the effect of the parameter on the optical absorption.

As shown in this chapter, photothermal deflection spectroscopy has proven to be a powerful tool for the investigation of very small optical absorptions. By overcoming the inherent limitations of conventional absorption techniques, PDS enables the direct and reliable determination of the energy and number of defects in hydrogenated amorphous silicon. Furthermore, it is an excellent tool for the characterization of material parameters such as doping concentration, defect level, and film homogeneity.

As to future directions, an obvious extension of the work reviewed in this chapter is the study of intrinsic defects and of other impurities. Another possibility is the investigation of the effects of alloying amorphous silicon with other materials such as germanium, carbon, or tin. Photothermal deflection spectroscopy is a unique tool for probing non-radiatiave transitions. When combined with luminescence studies, a complete picture of the branching ratios of radiative and non-radiative de-excitation should emerge. The study of the nature of defects in microcrystalline and of CVD deposited silicon is also a possible direction for future research.

Given the relative ease with which PDS can be performed, this technique has the potential of becoming an important addition to the tools employed in materials characterization, process control, and device diagnostics.

ACKNOWLEDGEMENTS

It is a pleasure to acknowledge the contributions of A.C. Boccara and D. Fournier to the development of photothermal deflection spectroscopy. This work was supported by the Assistant Secretary for Conservation and Renewable Energy, Photovoltaic Systems Division of the Department of Energy under Contract No. DE-AC03-76SF00098, and by the Solar Energy Research Institute Contract No. XJ-0-9079-1.

REFERENCES

1. Mott, N.F. (1979). "Electronic Processes in Non-Crystalline Materials," 2nd ed. (Oxford University Press, Oxford).

2. Cody, G., Wronski, C.R., Abeles, B., Stephens, R., and Brooks, B., (1980). Solar Cells *2*, 227.

3. Abeles, B., Wronski, C.R., Tiedje, T., and Cody, G.D., (1980). Solid State Commun. *36*, 537.

4. Tsai, C.C., and Fritzsche, F., (1979). Solar Energy Mat. *1*, 29.

5. Freeman, E.C., and Paul, W., (1979). Phys. Rev. B *20*, 716.

6. Zanzucchi, P.J., Wronski, C.R., and Carlson, D.E., (1977) J. Appl Phys. *48*, 5228.

7. Connell, G.A.N., and Pawlik, J.R., (1976). Phys. Rev. B *13*, 787.

8. Wronski, C.R., Abeles, B., Tiedje, T., and Cody, G.D., (1982). Solid State Commun. *44*, 1423.

9. Crandall, R.S., (1980). Phys. Rev. Lett. *44*, 749 (1980); Solar Cells, *2*, 319.

10. Moddel, G., Anderson, D.A., Paul, W., (1980). Phys. Rev. B *22*, 1918.

11. Loveland, R.J., Spear, W.E., and Al-Sharbaty, A., (1973). J. Non-Cryst. Sol. *11*, 55.

12. Jackson, W.B., Amer, N.M., Boccara, A.C., and Fournier, D. (1981). Appl. Opt. *20*, 1333.

13. Boccara, A.C., Fournier, D., Jackson, W.B., and Amer, N.M., (1980). Opt. Lett. *5*, 377.

14. Boccara, A.C., Fournier, D., and Badoz, J., (1980). Appl. Phys. Lett. *36*, 130.

15. Yasa, Z.A., Jackson, W.B., and Amer, N.M., (1982). Appl. Opt. *21*, 21.

16. Silicon Detector Corp., Newbury Park, California.

17. Parker, G., (1973). Appl. Opt. *12*, 2974.

18. Jackson, W.B., and Amer, N.M. (1981). In "Tetrahedrally Bonded Amorphous Semiconductors," R.A. Street, D.K. Bieglson, and J.C. Knights, Edits., AIP Conf. Proc. No. 73 (AIP, New York), p. 263.

19. Jackson, W.B., and Amer, N.M., (1981). J. Phys. (Paris) *42*, C4-293.

20. Yamasaki, S., Hata, N., Yoshida, T., Oheda, H., Matsuda, A., Okushi, H., and Tanaka, K., (1981). J. Phys. (Paris) *42*, C4-297.

21. Jackson, W.B., and Amer, N.M., (1982). Phys. Rev. B *25*, 5559.

22. Brodsky, M.H., Cardona, M., and Cuomo, J.J., (1977). Phys. Rev. B *16*, 3556.

23. Dexter, D.L., (1956). Phys. Rev. *101*, 48.

24. Freeman, E.C., and Paul, W. (1978). Phys. Rev. B *18*, 4288.

25. Street, R.A., (1981). Phys. Rev. B *24*, 969.

26. Brodsky, M.H., Kaplan, D.M., and Ziegler, J.F., (1972). In "Proceedings of the 11th International Conference on the Physics of Semiconductors, Warsaw-1972," edited by the Polish Academy of Sciences (Elsevier, Amsterdam), p. 529.

27. Street, R.A., (1982). Phys. Rev. Lett. *49*, 1187; and references therein.

28. Jackson, W.B., (1982). Solid State Commun. *44*, 477.

29. Dersch, H., Stuke, J., and Beichler, J., (1981). Phys. Stat. Solidi (b) *105*, 265.

30. Knights, J.C., Biegelsen, D.K., and Solomon, I., (1977). Solid State Commun. *22*, 133.

31. Ast, D.G., and Brodsky, M.H., (1980). Philos. Mag. B *24*, 273.

32. Fritzsche, H., (1980). Solar Cells *2*, 289.

33. Solomon, I., Dietl, T., and Kaplan, D., (1978). J. Phys. (Paris) *39*, 1241.

34. Jackson, W.B., Biegelsen, D.K., Nemanich, R.J., and Knights, J.C., (1983). Appl. Phys. Lett. *42*, 105.

35. Staebler, D.L., and Wronski, C.R., (1980). J. Appl. Phys. *51*, 3262.

36. Staebler, D.L., and Wronksi, C.R., (1977). Appl. Phys. Lett. *31*, 292.

37. Amer, N.M., Skumanich, A., and Jackson, W.B., (1983). Physica (Utrecht) *117B* and *118B*, 897.

38. Dersch, H., Stuke, J., and Beichler, J., (1981). Appl. Phys. Lett. *38*, 456.

39. Tiedje, T., Cebulka, J.M., Morel, D.L., and Abeles, B., (1981). Phys. Rev. Lett. *46*, 1425.

40. Wake, D.R., and Amer, N.M., (1983). Phys. Rev. B *27*, 2598.

41. Skumanich, A., Wake, D.R., and Amer, N.M. (1983). Bull. Amer. Phys. Soc. *28*, 257.

42. Lang, D.V., Cohen, J.D., Harbison, J.P., and Sergent, A.M., (1982). Appl. Phys. Lett. *40*, 474.

43. Skumanich, A., Amer, N.M., and Jackson, W.B., (submitted).

44. Carlson, D.E., (1982). Solar Energy Mat. *8*, 129.

45. Staebler, D.L., Crandall, R.S., and Williams, R., (1981). Appl. Phys. Lett. *39*, 733.

46. Carlson, D.E., (1982). J. Vac. Sci. Technol. *20*, 290.

47. Jackson, W.B., Nemanich, R.J., and Amer, N.M., (1983). Phys. Rev. B *27*, 4861.

48. Pierce, D.J., and Spicer, W.E., (1972). Phys. Rev. B *5*, 3017.

FIGURE CAPTIONS

Fig. 1: The experimental arrangement.

Fig. 2: The substrate-temperature dependence of gap-state absorption. Undoped material.

Fig. 3: The dependence of gap-state absorption on deposition power. Undoped material.

Fig. 4: The dependence of gap-state absorption on the type and level of doping. (a) PH_3—doping concentration: (1) 10^{-2}, (2) 10^{-3}, (3) 3×10^{-4}, (4) 10^{-5}, and (5) 10^{-6}; (b) B_2H_6—doping concentration: (6) 10^{-3}, (7) 3×10^{-4}, and (8) 10^{-4}, (9) 10^{-5}; (c) Compensated material: all samples have $10^{-3}PH_3$ and the B_2H_6 concentrations are (10) 2×10^{-4}, (11) 4×10^{-4}, (12) 2×10^{-3}, and (13) 4×10^{-3}. All doping concentrations refer to gas phase concentration. Substrate temperature = 230°C and the rf deposition power is 2 W.

Fig. 5: The correlation between the number of defects deduced from PDS and ESR. Undoped material.

Fig. 6: The correlation between the number of defects deduced form PDS and from luminescence quenching.

Fig. 7: Calculated and PDS-deduced absorption for undoped and phosphorous-doped materials.

Fig. 8: Photon energy dependence of the absorption for phosphorous-doped and undoped material. The doped curves have been shifted to the right by 0.35 eV and multiplied by a factor of 3.

Fig. 9: Thickness dependence of the absorption in undoped a-Si:H.

Fig. 10: The effect of illumination on the absorption spectrum of undoped a-Si:H.

Fig. 11: The dependence of ΔN_s on doping concentration.

Fig. 12: The dependence of ΔN_s on N_s for doped and undoped materials.

Fig. 13: The correlation between the Urbach edge energy and the ESR-deduced spin density.

Fig. 14: The correlation between photoinduced and PDS-deduced optical absorption for undoped material with varying defect density.

Fig. 15: Types of photoconductivity: (a) secondary gap photoconductivity (SSPC); (b) secondary forward-bias photoconductivity (SPPC); and (c) primary reverse-bias photoconductivity (PPPC).

Fig. 16: The dependence of constant-generation-rate photoconductivity and absorptance on photon energy. ○—PDS; Δ—SSPC; □—SPPC; ■—PPPC.

Fig. 17: $\eta\mu\tau$ derived from photoconductivity and absorptance. Δ—$(\eta\mu\tau)_e + (\eta\mu\tau)_h$ from SSPC; □—$(\eta\mu\tau)_e$ from SPPC. The curves are offset vertically for clarity.

Fig. 18: $(\eta\mu\tau)_h$, relative to the value at 2.0 eV, as a function of photon energy.

Fig. 19: Density-of-states for undoped and phosphorous-doped a-Si:H. E_F denotes the Fermi level for single occupancy.

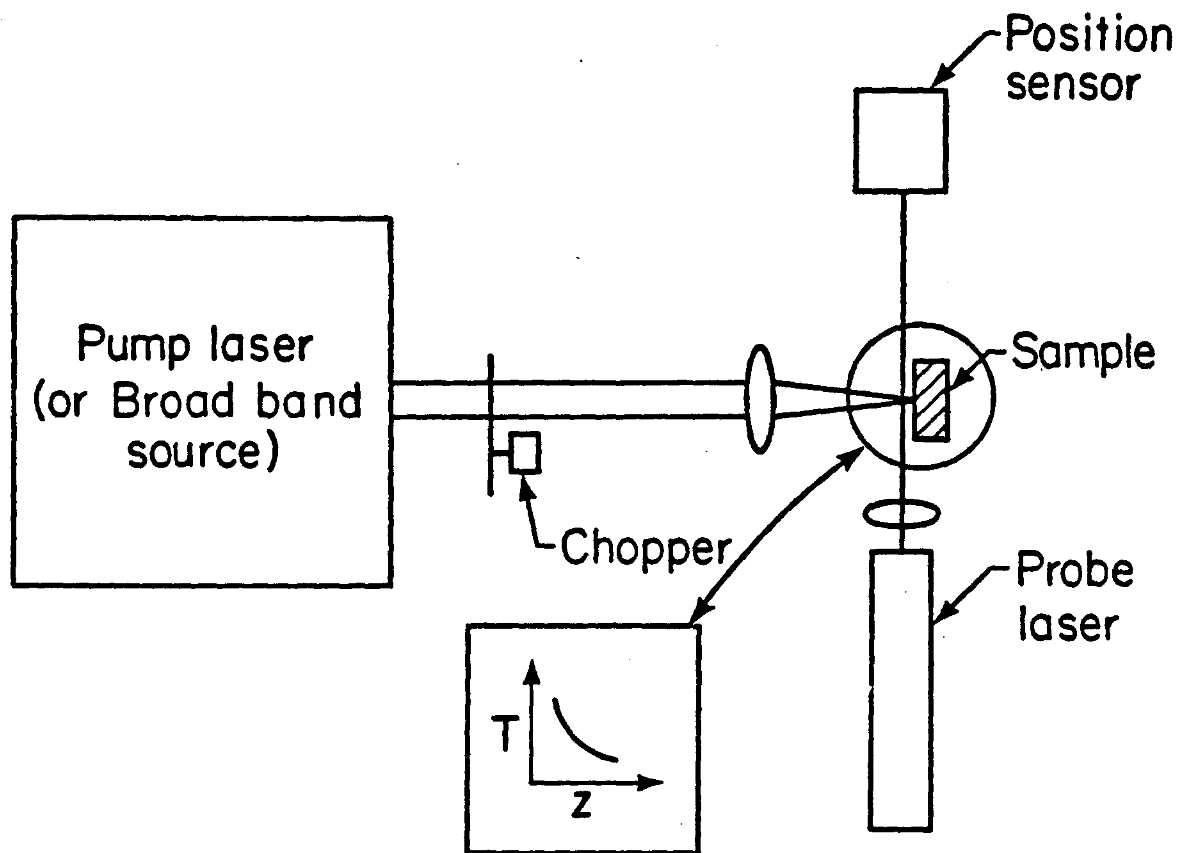

Fig. (1)

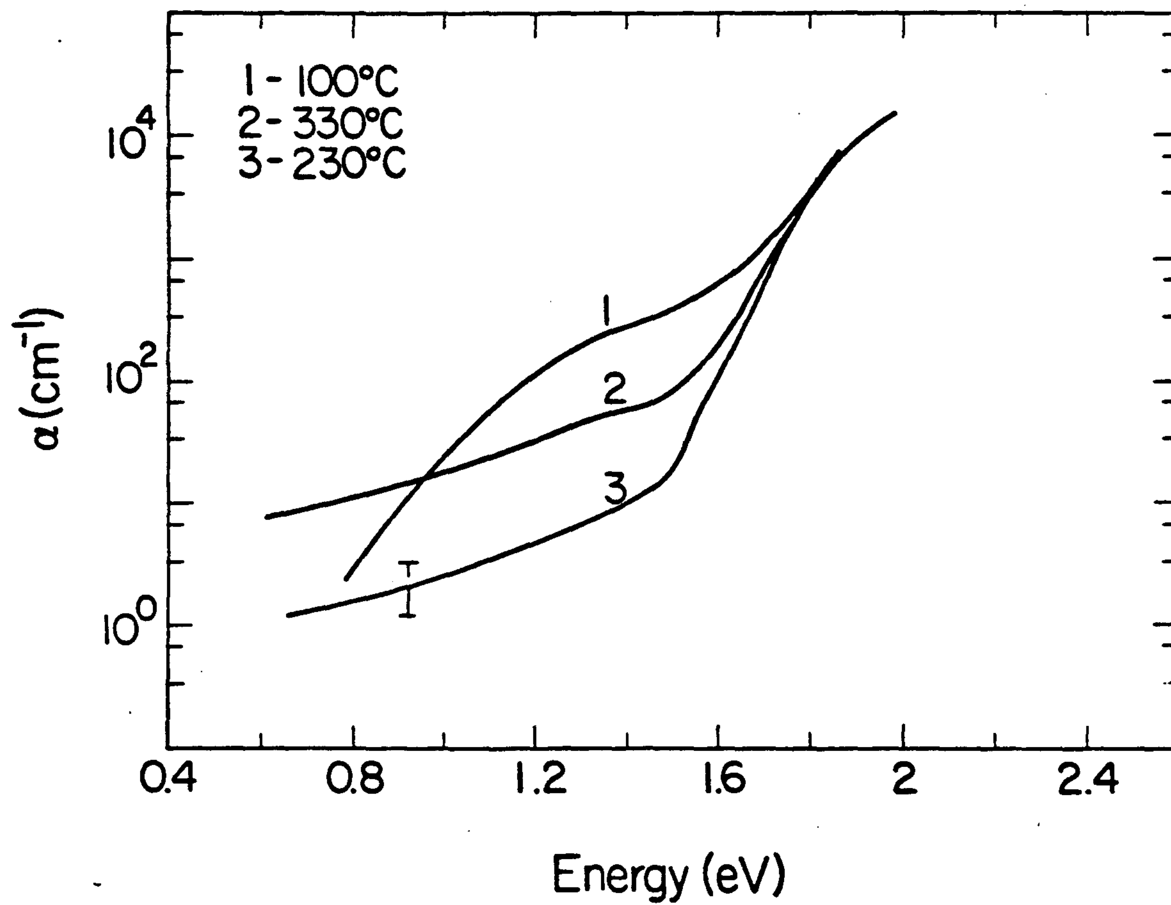

Fig. (2)

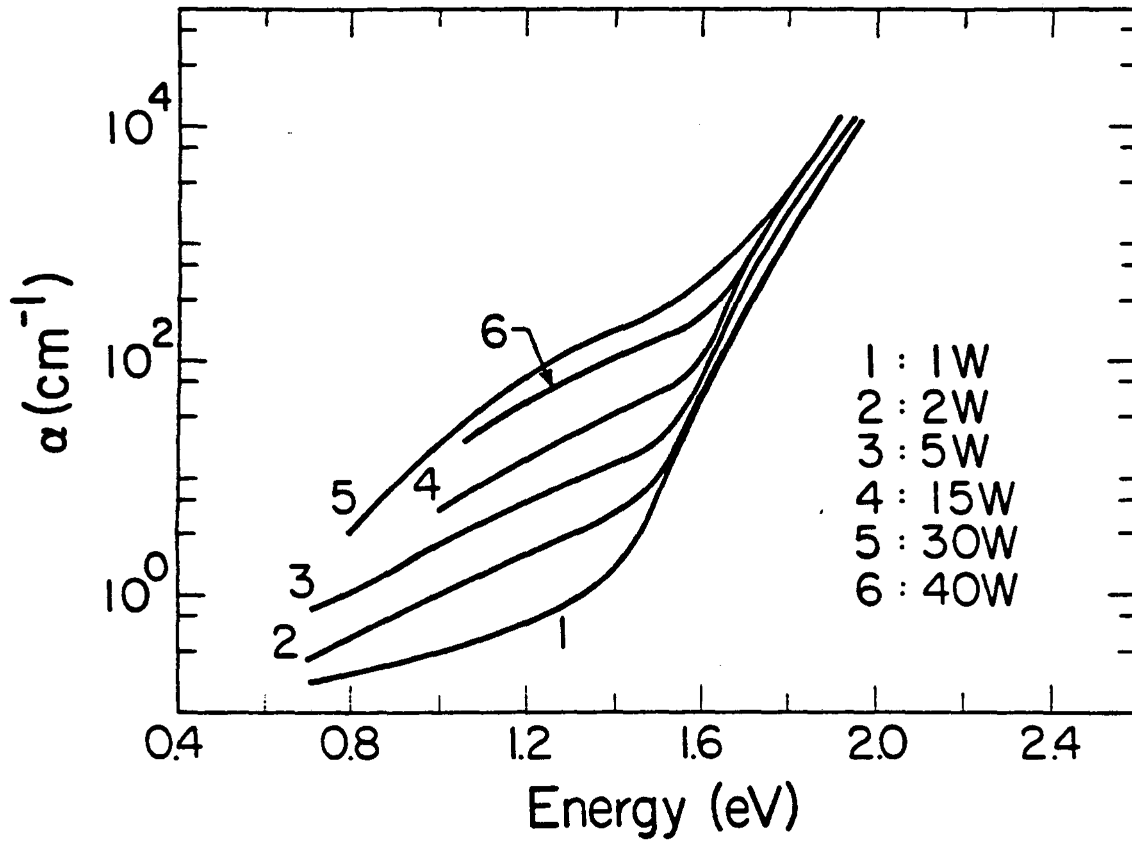

Fig. (3)

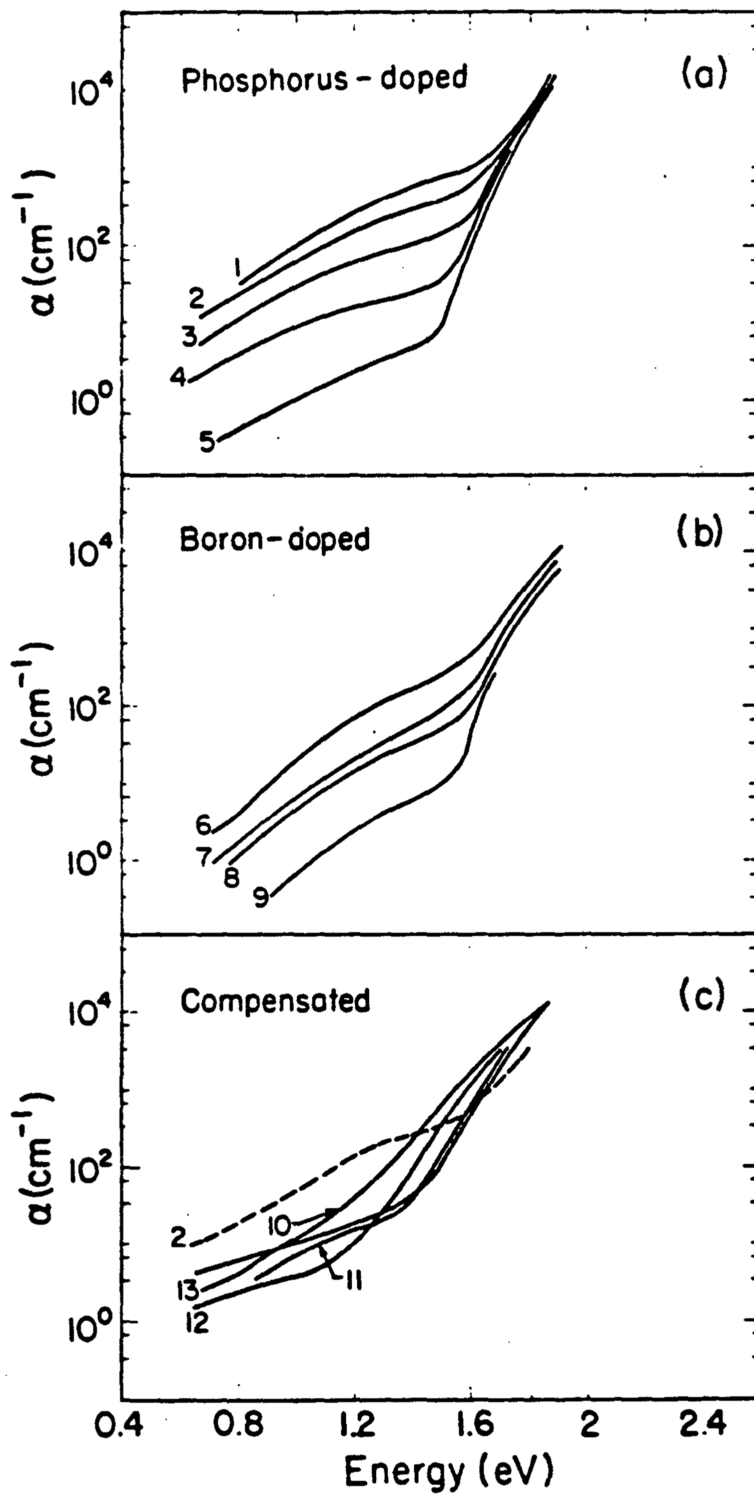

Fig. (4)

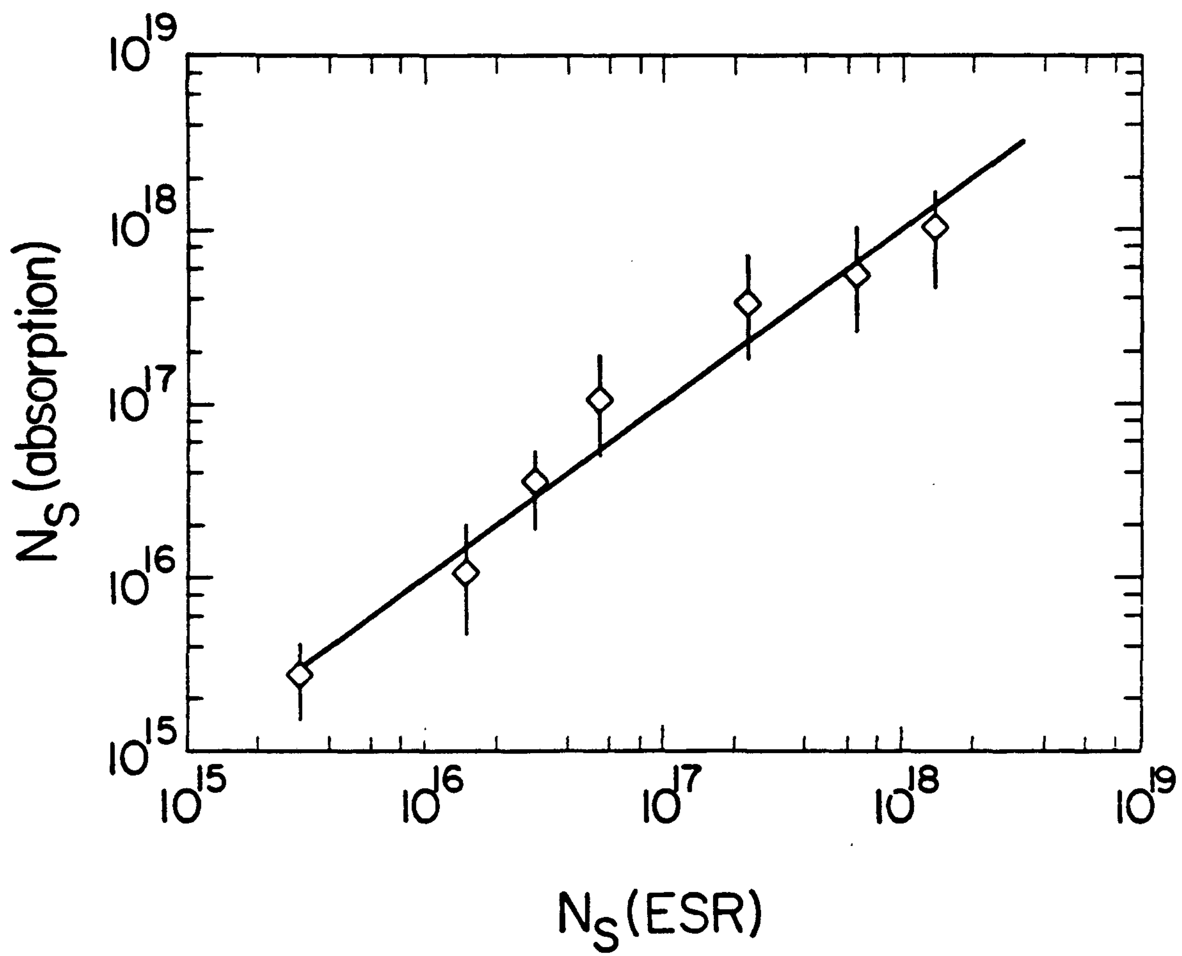

Fig. (5)

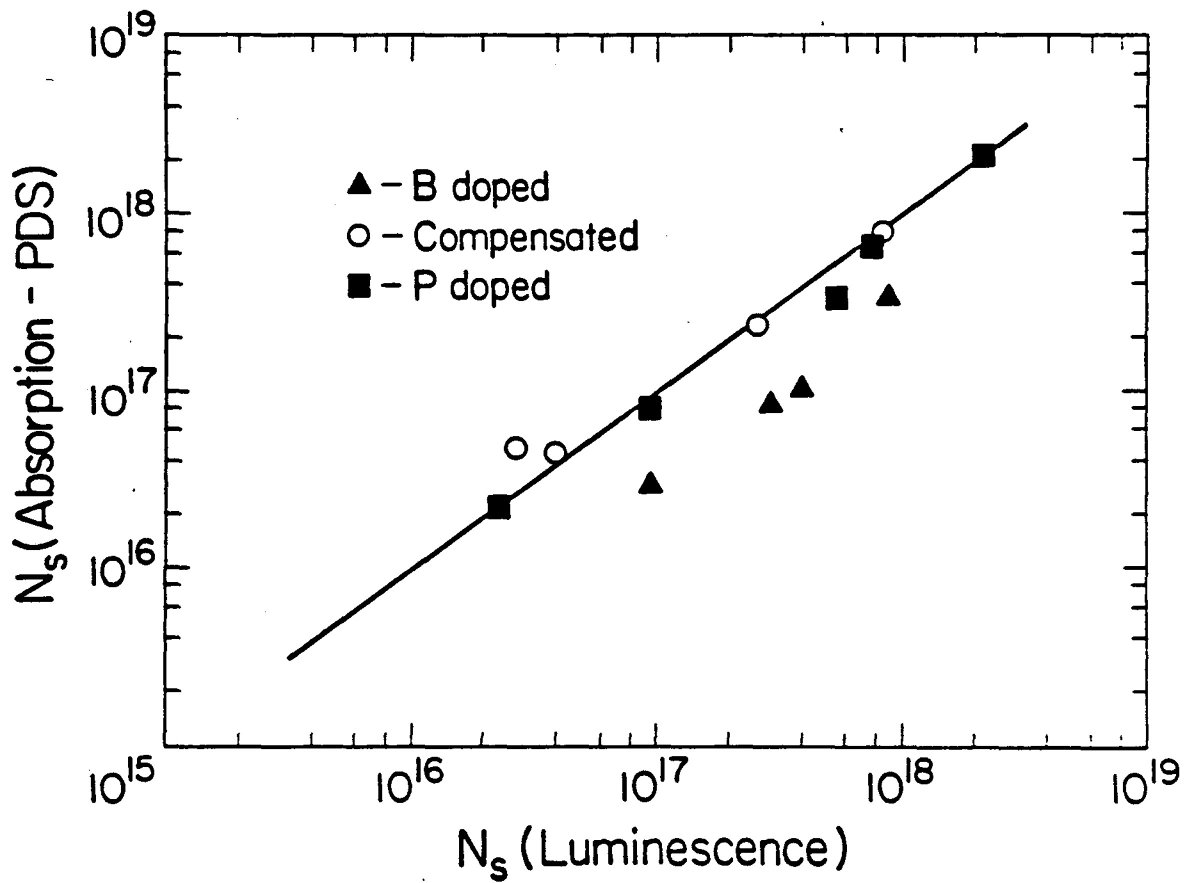

Fig. (6)

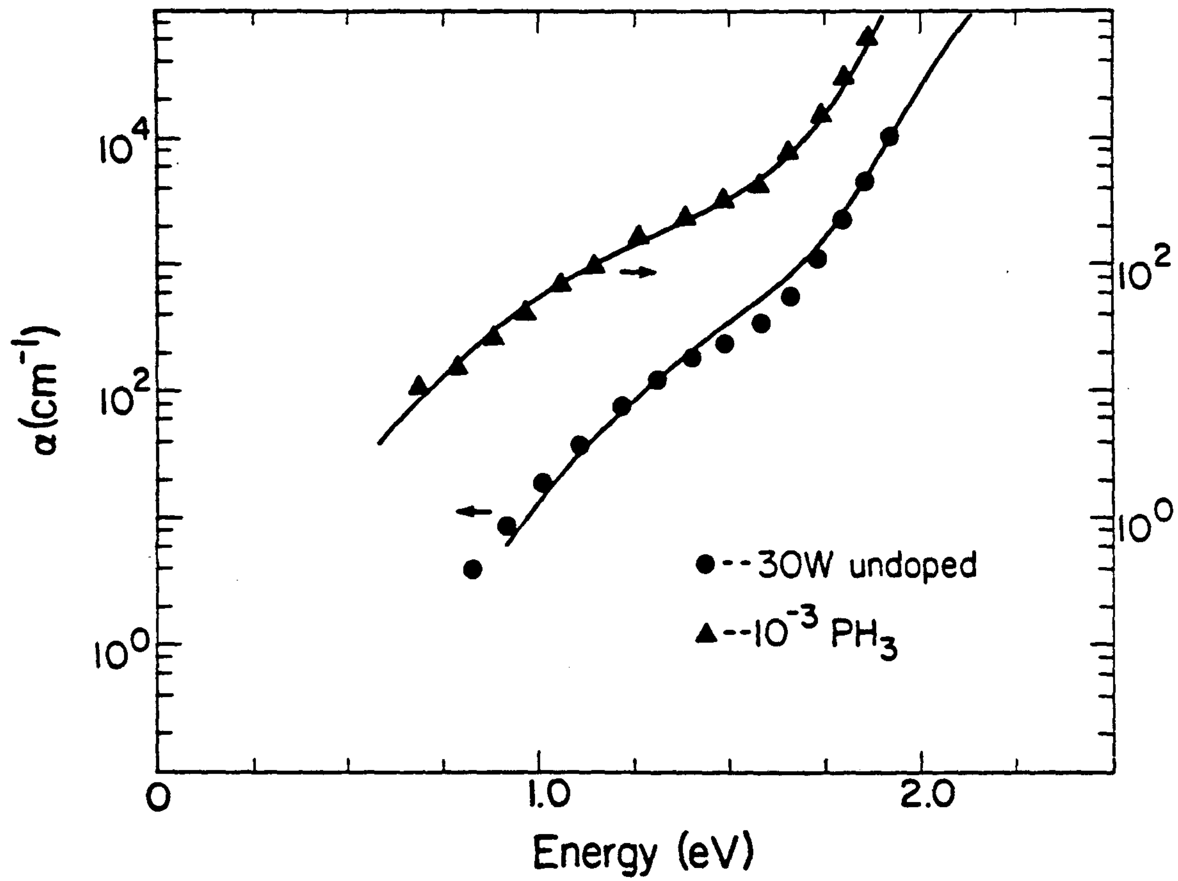

Fig. (7)

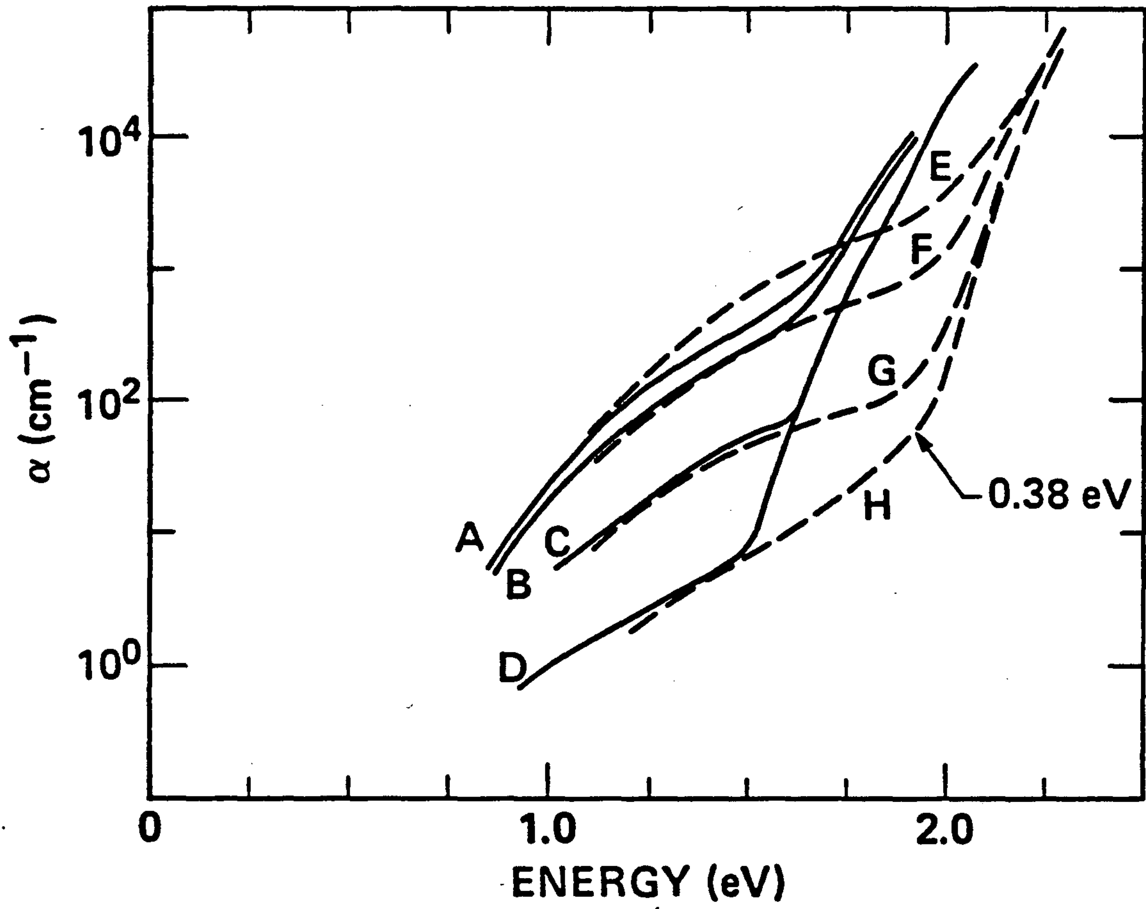

Fig. (8)

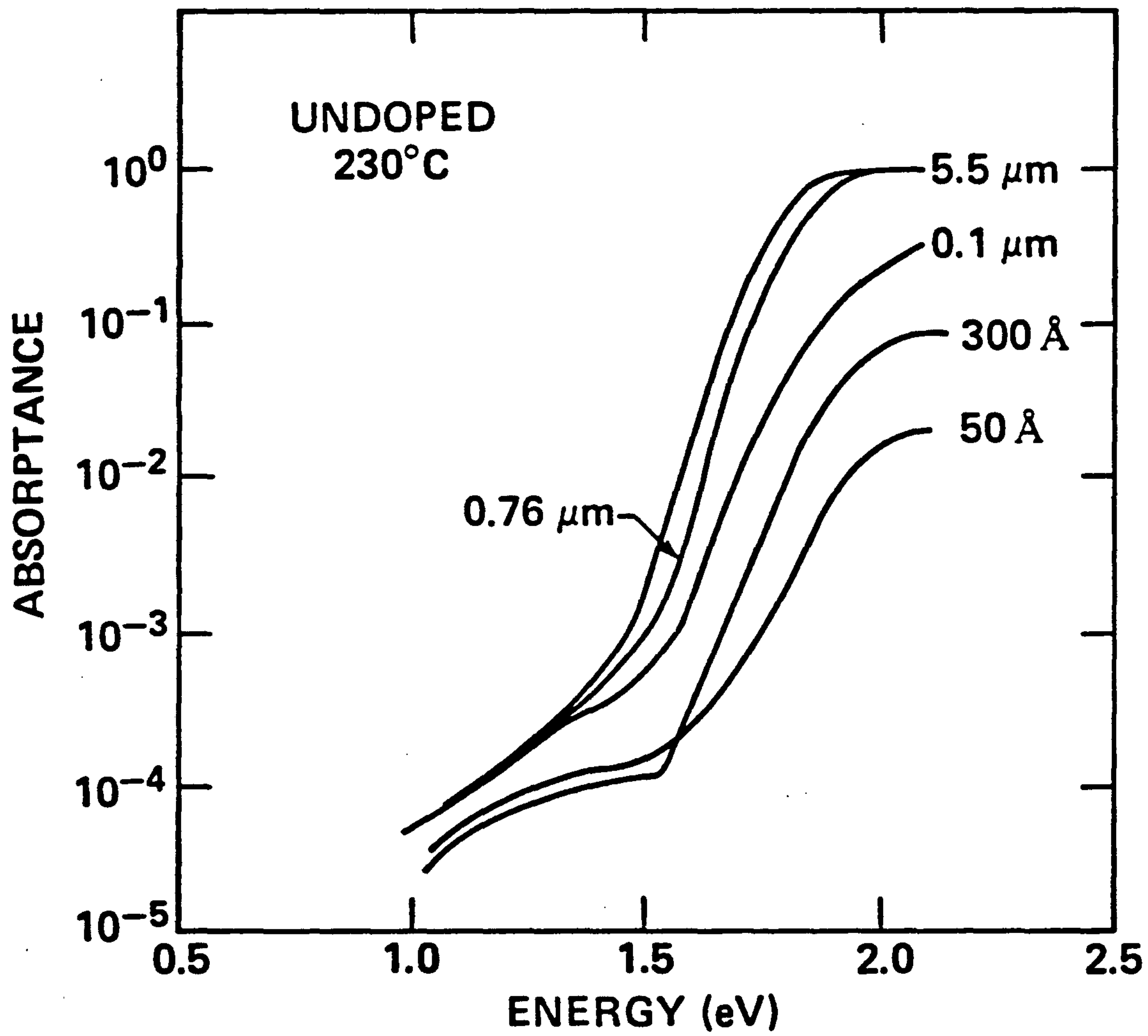

XBL 835-9668

Fig. (9)

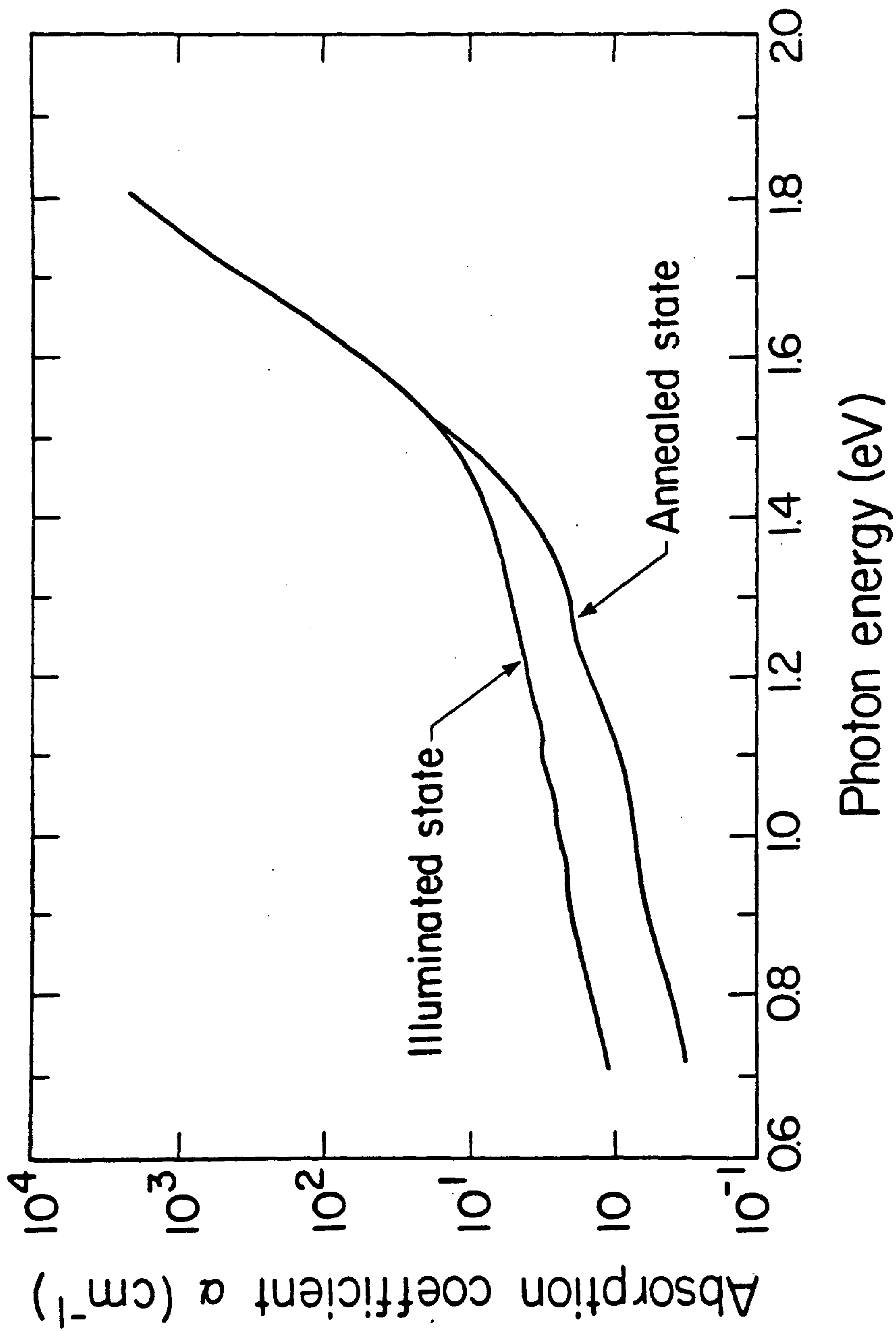

Fig. (10)

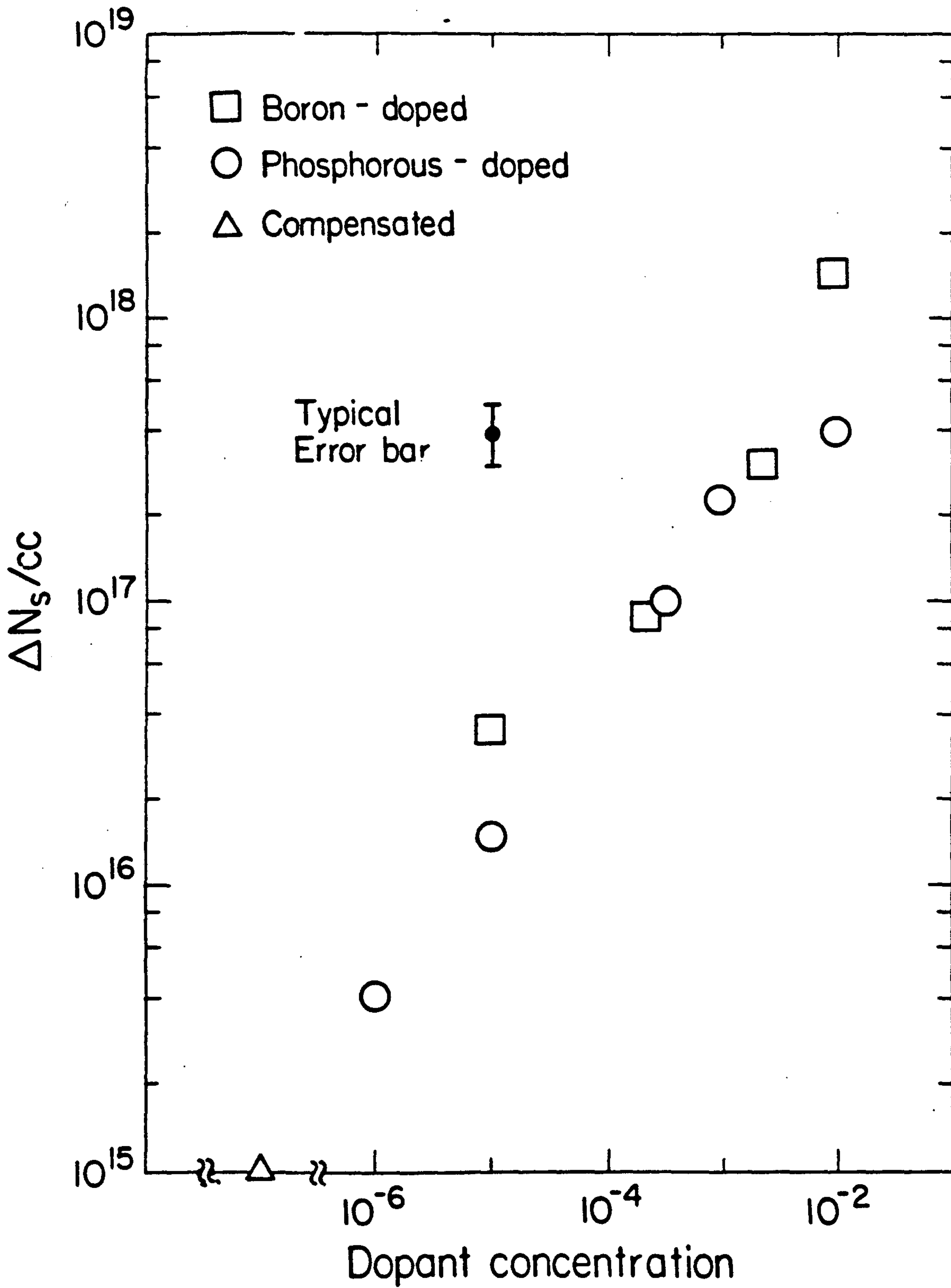

Fig. (11)

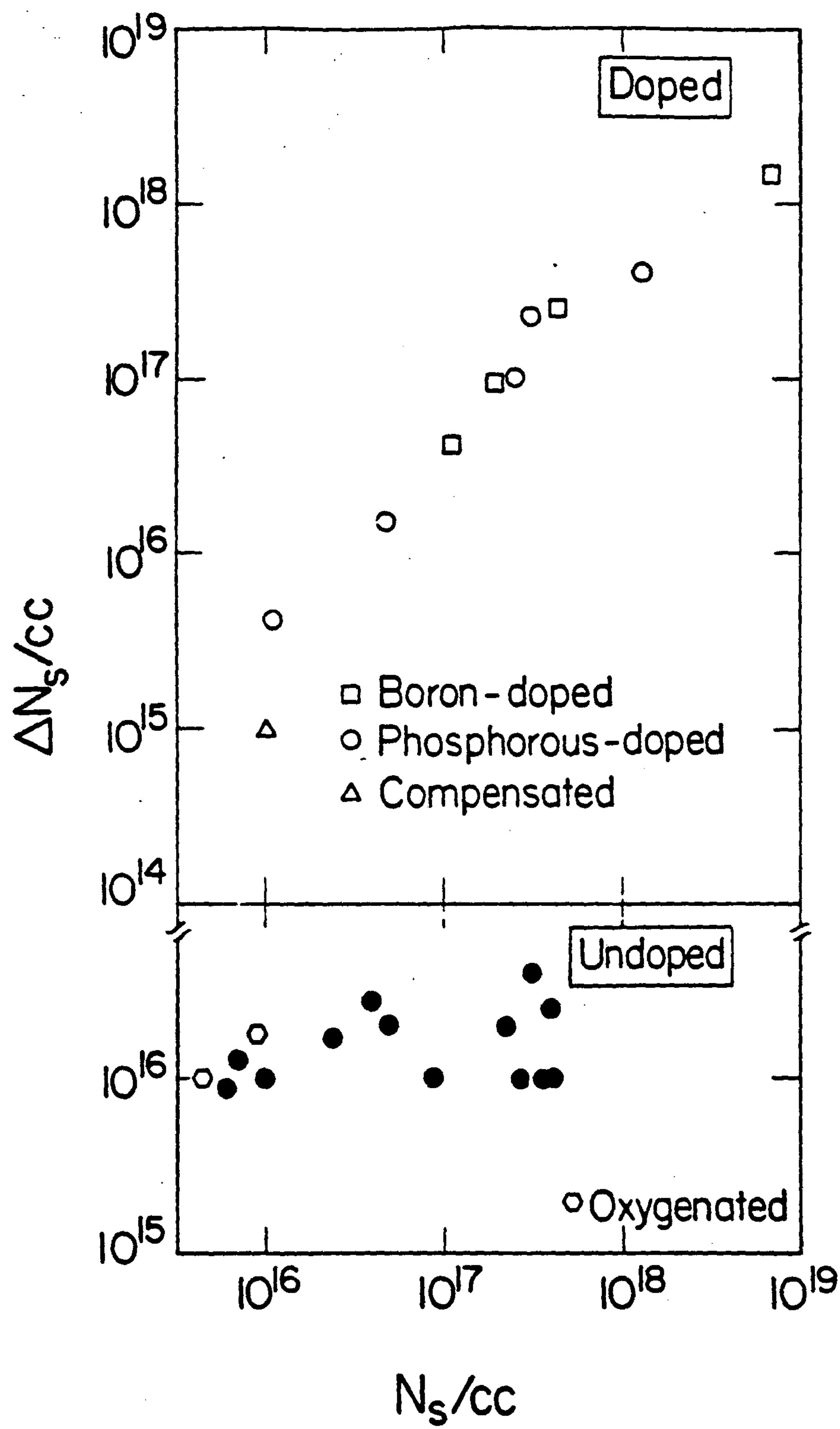

Fig. (12)

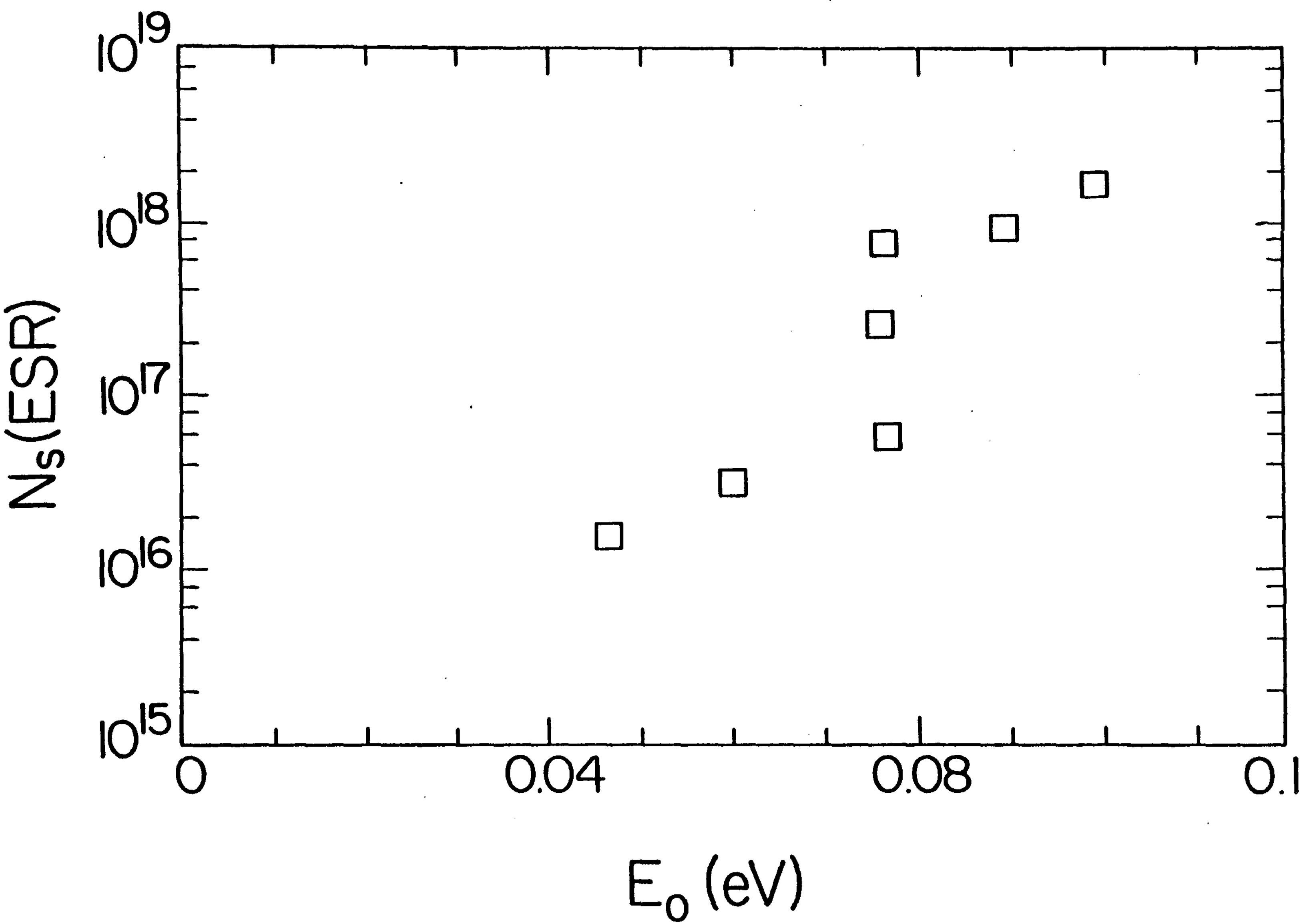

Fig. (13)

XBL 836-2670

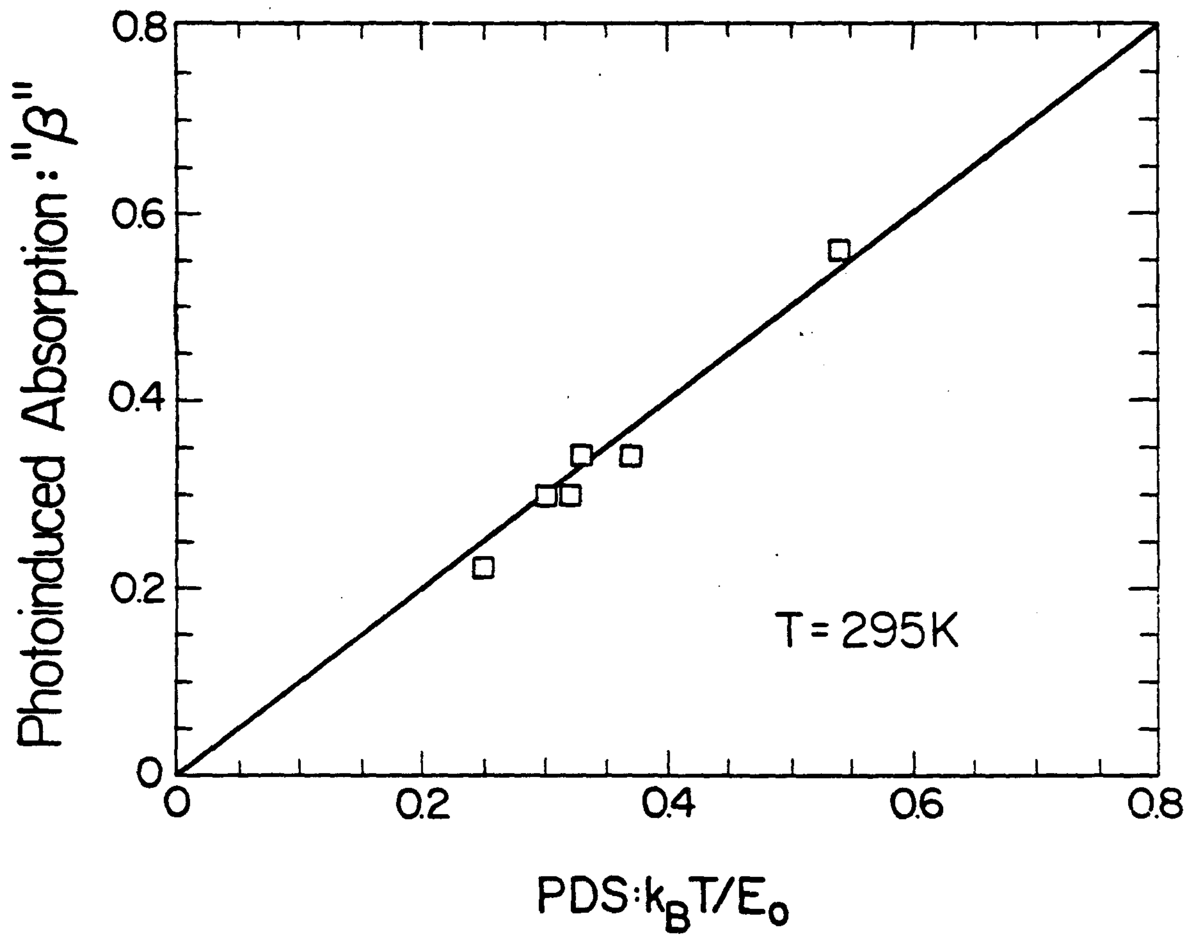

XBL 836-2673

Fig. (14)

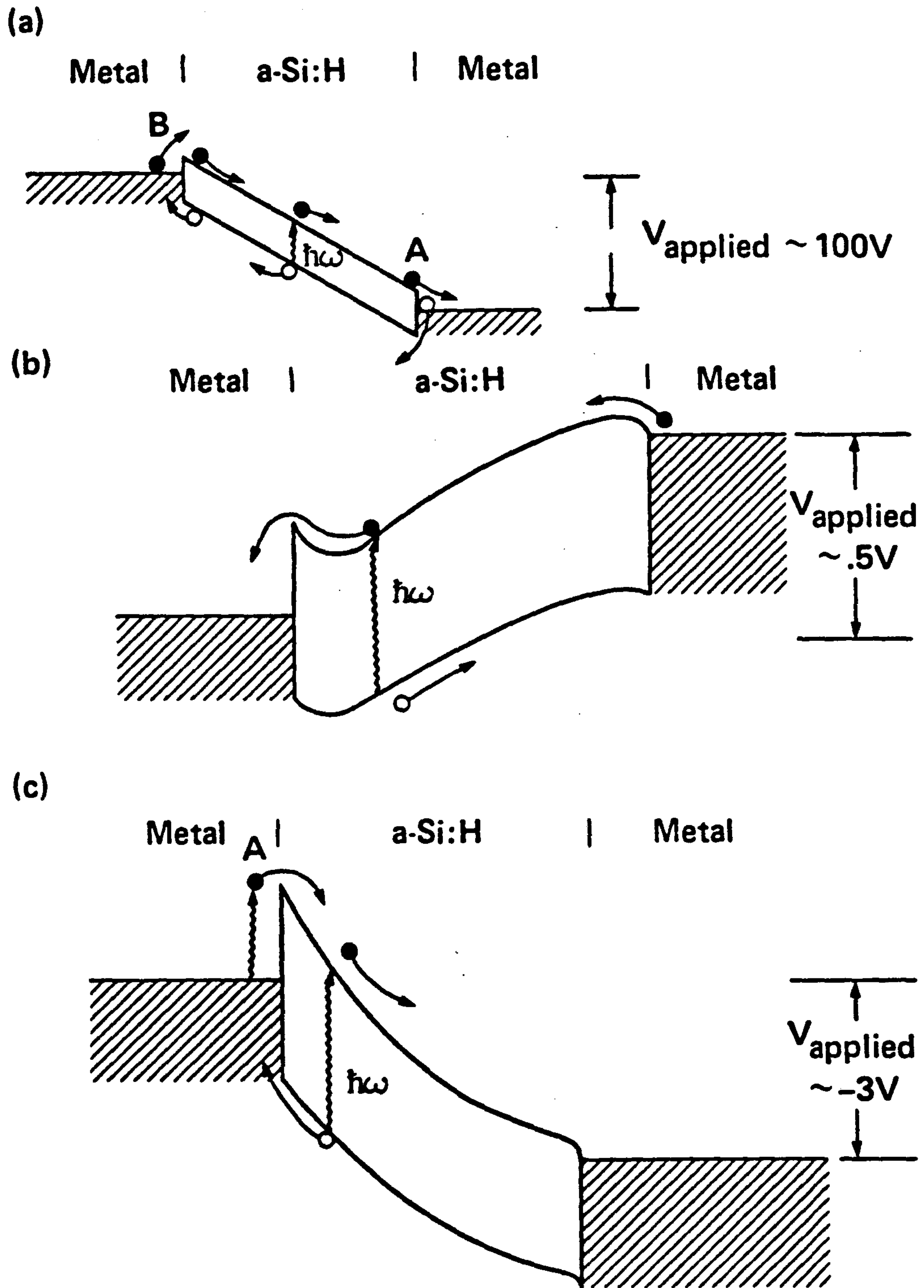

Fig. (15)

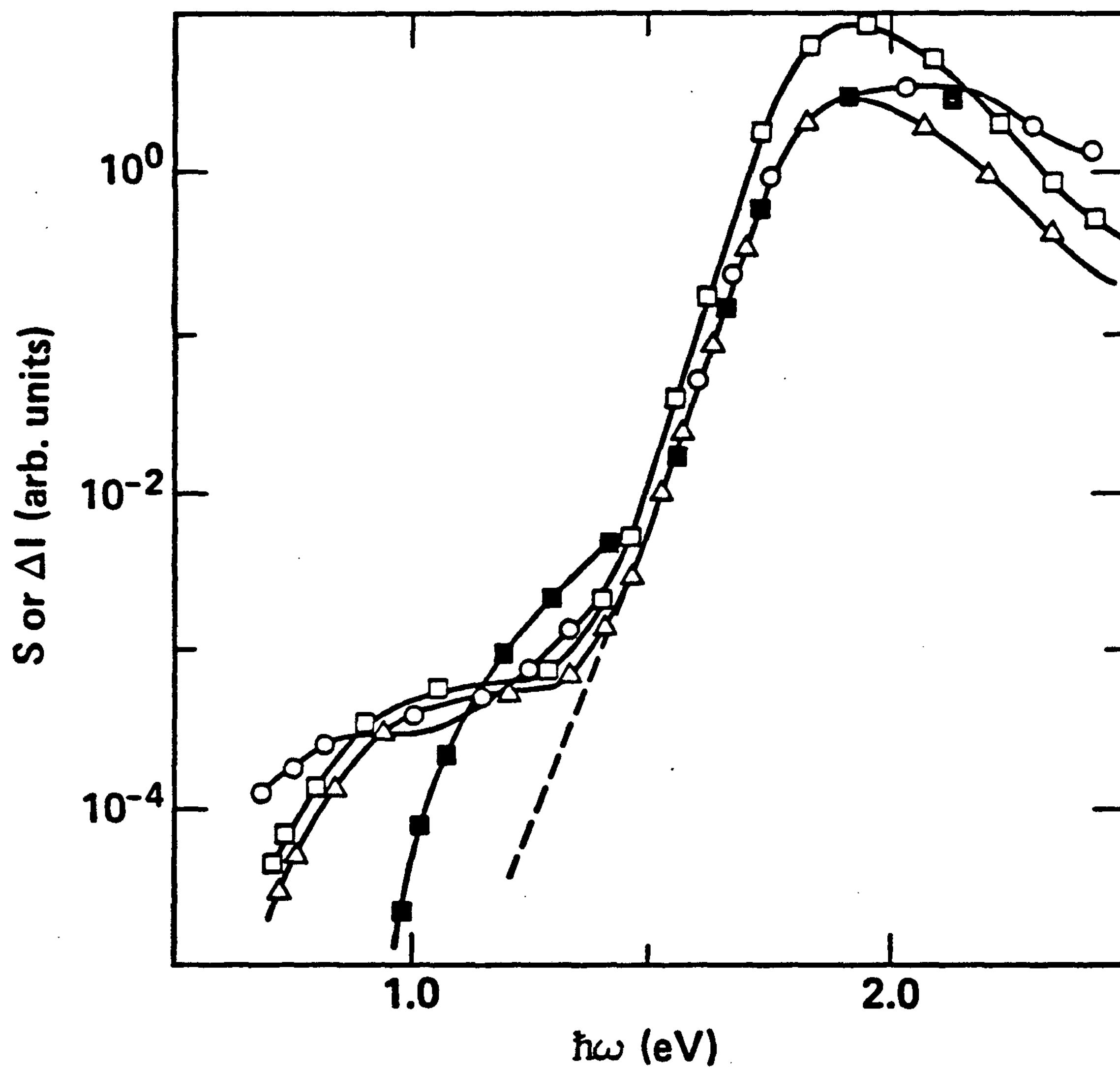

XBL 835-9675

Fig. (16)

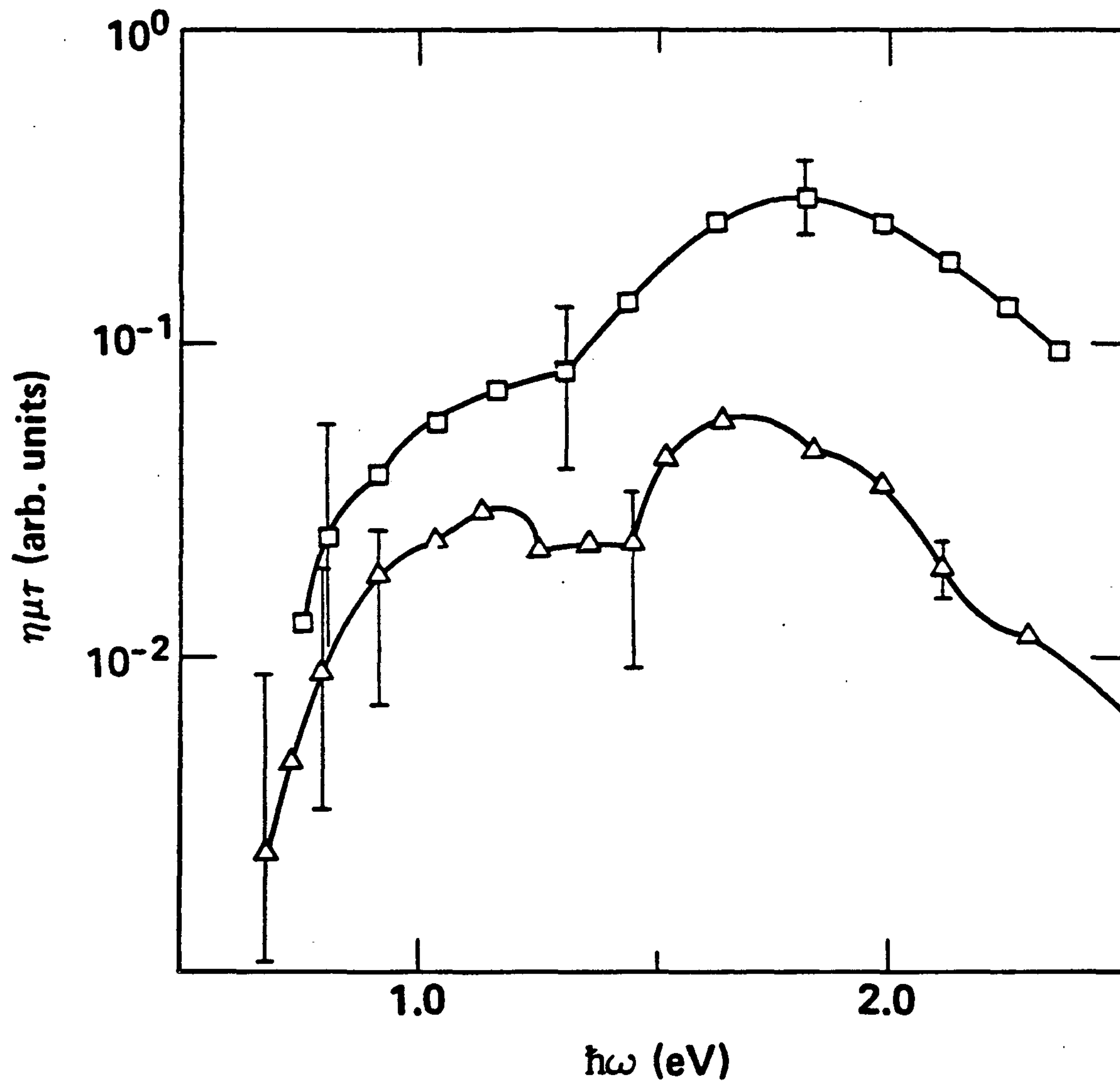

XBL 835-9672

Fig. (17)

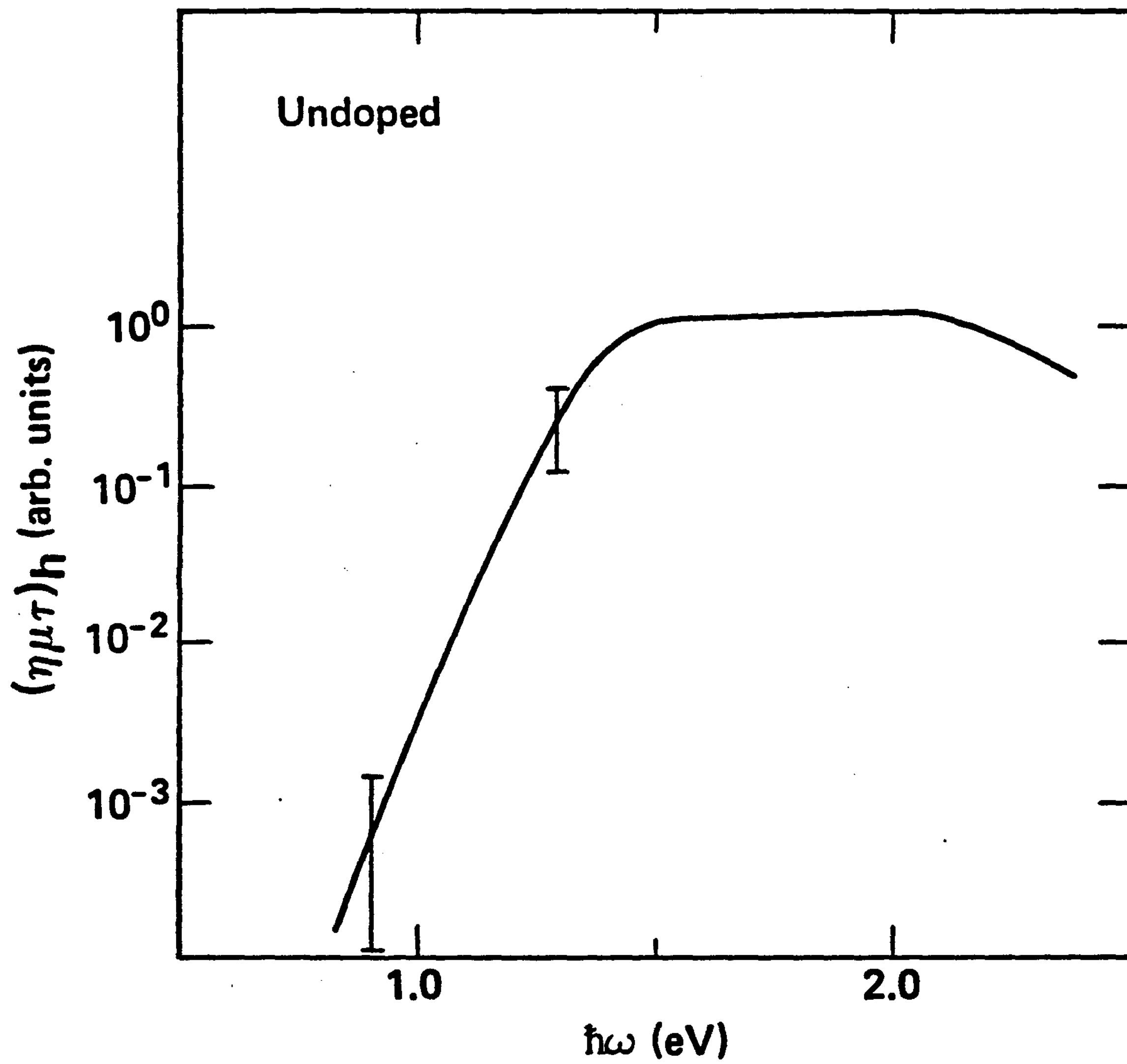

Fig. (18)

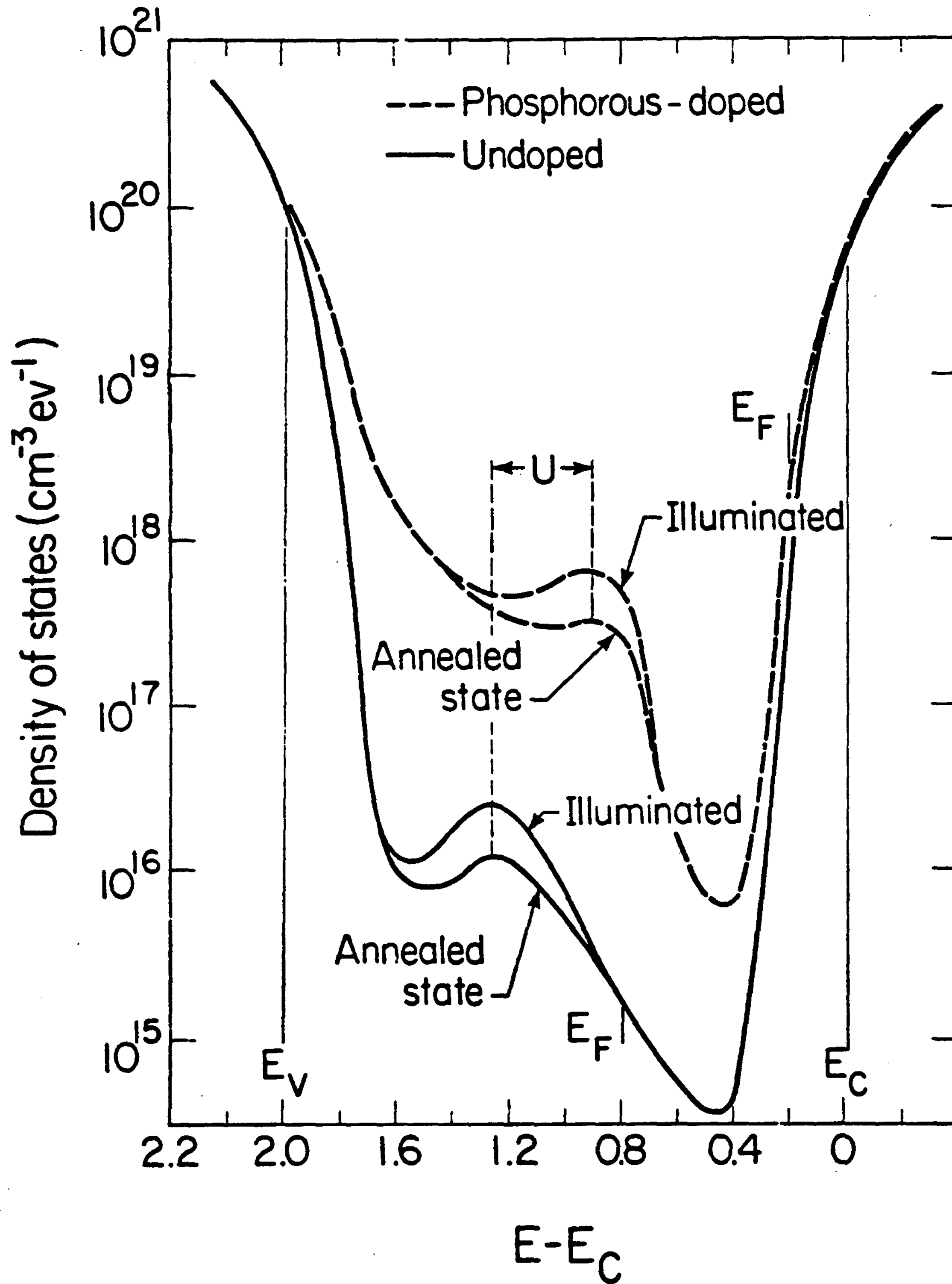

Fig. (19)

This report was done with support from the Department of Energy. Any conclusions or opinions expressed in this report represent solely those of the author(s) and not necessarily those of The Regents of the University of California, the Lawrence Berkeley Laboratory or the Department of Energy.

Reference to a company or product name does not imply approval or recommendation of the product by the University of California or the U.S. Department of Energy to the exclusion of others that may be suitable.

TECHNICAL INFORMATION DEPARTMENT
LAWRENCE BERKELEY LABORATORY
UNIVERSITY OF CALIFORNIA
BERKELEY, CALIFORNIA 94720